Neuregulin-1 regulates cardiomyocyte dynamics, cell cycle progression, and maturation during ventricular chamber morphogenesis

Joaquim Grego-Bessa[1,2], Paula Gómez-Apiñaniz[1,2], Belén Prados[1,2], Manuel José Gómez[3], Donal MacGrogan[1,2,*] & José Luis de la Pompa[1,2,*]

Centro Nacional de Investigaciones Cardiovasculares Carlos III (CNIC), Melchor Fernández Almagro 3, 28029 Madrid, SPAIN.

[2] CIBER de Enfermedades Cardiovasculares, Madrid, SPAIN

[3] Bioinformatics Unit, CNIC, Madrid SPAIN

[*] Corresponding authors: dmacgrogan@cnic.es, jlpompa@cnic.es. Phone: +34-620-936633

BACKGROUND: Cardiac ventricles are essential for providing the contractile force of the beating heart throughout life. How the primitive endocardium-layered myocardial projections called trabeculae form and mature into the adult ventricles is of great interest for fundamental biology and regenerative medicine. Trabeculation is dependent on the signaling protein Neuregulin-1 (Nrg1). However, the mechanism of action of Nrg1 and its role in ventricular wall maturation are poorly understood.

METHODS: In this study we investigated the functions and downstream mechanisms of Nrg1 signaling during ventricular chamber development using confocal imaging, transcriptomics, and biochemical approaches in mice with conditional cardiac-specific inactivation or overexpression of Nrg1.

RESULTS: Analysis of cardiac-specific-*Nrg1* mutant mice showed that the transcriptional program underlying cardiomyocyte-oriented cell division and trabeculae formation depends on endocardial Nrg1 to myocardial ErbB2 signaling and pErk activation. Early endothelial loss of Nrg1 and below normal pErk activation diminished cardiomyocyte Pard3 and Crumbs2 protein, and altered cytoskeletal gene expression and organization. These changes were associated with aberrant expression of genes involved in mitotic spindle organization and a directional shift from perpendicular to parallel/obliquely-oriented cardiomyocyte division. Further analysis indicated that Nrg1 is required for trabecular growth and ventricular wall thickening by regulating an epithelial-to-mesenchyme transition (EMT)-like process in cardiomyocytes involving migration, adhesion, cytoskeletal actin turnover, and timely progression through the cell cycle G2/M phase. Ectopic cardiac Nrg1 overexpression and high pErk signaling caused S-phase arrest, maintained high EMT-like gene expression and prolonged trabeculation, blocking compact myocardium maturation. Likewise, alterations of myocardial trabecular patterning resulting from above- or below-normal Nrg1-dependent pErk activation were concomitant with disorganization of the sarcomere actin cytoskeleton. The Nrg1 loss- and gain-of-function transcriptomes were enriched for yes-associated protein-1 (Yap1) gene signatures, identifying Yap1 as a potential downstream effector. Biochemical and imaging data showed that pErk activation and nuclear-cytoplasmic distribution of Yap1 during trabeculation are dependent on Nrg1.

CONCLUSIONS: These data establish the Nrg1-ErbB2/4-pErk axis as a crucial regulator of cardiomyocyte cell cycle progression and migration during ventricular development. Moreover, our data identify a Nrg1-dependent signaling cascade that could be leveraged for future cardiac regenerative therapies.

Key Words: Ventricular development, trabeculation, apico-basal polarity, oriented cell division, compaction, ventricular conduction system, actin cytoskeleton, EMT-like, cell cycle, Nrg1, ErbB2, Erk, Yap1.

60 **Nonstandard Abbreviations and Acronyms**

61 4-OHT, 4-hydroxytamoxifen
62 A-B polarity, apico basal polarity
63 CM, compact myocardium
64 EMT-like, epithelial-mesenchymal transition-like
65 ErbB2/4, erb-b2 receptor tyrosine kinase 2/4
66 Erk, extracellular signal regulated MAP kinase
67 GOF, gain-of-function
68 GSEA, gene set enrichment analysis
69 IF, immunofluorescence
70 LOF, loss-of-function
71 Nrg1, neuregulin-1
72 OCD, oriented cell division
73 OE, overexpression
74 SMA, smooth muscle actin
75 SM22, smooth muscle cell-specific cytoskeletal protein
76 TM, trabecular myocardium
77 VCS, ventricular conduction system
78 Yap1, yes1-associated transcriptional regulator
79

Novelty and Significance

WHAT IS KNOWN?

- Myocardial trabeculae play important roles in ventricular chamber growth, development of the conduction system, and formation of the coronary arteries.
- Trabeculae are formed through oriented cell division (OCD), and their growth is driven by directional migration.
- The membrane glycoprotein Neuregulin-1 (Nrg1) mediates cell-cell signaling and is essential for trabecular development.

WHAT NEW INFORMATION DOES THIS ARTICLE CONTRIBUTE?

- Nrg1 signaling is essential for the expression of cardiomyocyte polarity genes and the organization of the cytoskeleton during the oriented cell division process underlying trabeculation.
- Nrg1 is required for the formation of the inner ventricular wall but not the coronaries.
- Nrg1 regulates motility and cell-cycle progression during ventricular wall growth.
- Ectopic expression of Nrg1 leads to excessive trabeculation of the myocardium and disrupts compaction.
- Nrg1 regulates ventricular patterning mediated by cytoskeletal dynamics and modulates pErk-dependent Yap1 S274 phosphorylation during trabeculation.
- Nrg1 is not required for ventricular compaction.

100 **Introduction**

101 Ventricular chamber development entails transient morphogenetic changes that include the formation
102 of trabeculae, their expansion and growth, and their subsequent incorporation into a compact muscular
103 wall. Fate-mapping and time-lapse live imaging in zebrafish has shown that trabeculae form by the
104 extrusion of cardiomyocytes and their radial extension along the inner curvature of the looping heart
105 and into the ventricular lumen [1-5]. In mice, trabeculation begins with oriented cell division (OCD)
106 perpendicular to the ventricular inner wall plane, and trabecular growth is driven by directional
107 migration from the outer (epicardial) layer toward the inner (endocardial) layers [6-8]. The process of
108 trabeculae coalescence forms a dense meshwork that maximizes ventricular surface area for nutrient
109 and gas exchange in the absence of a coronary circulation [9]. This meshwork later differentiates into a
110 specialized ventricular conduction system and is resolved by expansion of the compact myocardial
111 wall, with trapped endocardial cells giving rise to the coronary arteries [10-14].

112 Trabeculation defects or failed compaction in humans, manifests as hypertrabeculation or non-
113 compaction phenotypes [15]. Trabeculae thickening, decreased intertrabecular spacing, and
114 underdevelopment of the compact wall myocardium are defining morphological features of left
115 ventricular non-compaction cardiomyopathy [16]. This phenotype is observed in various conditions, that
116 have been associated with sarcomeric genes, cardiac contractility, calcium handling, and
117 developmental signaling pathways [17]. Conversely, acquired non-compaction or the appearance of
118 hypertrabeculation in trained athletes or during pregnancy, have been interpreted as
119 morphophysiological manifestations of increased hemodynamic load [18]. Moreover, genetic
120 association and Mendelian randomization studies have found an inverse relationship between the
121 complexity of trabecular morphology and the risk of cardiovascular disease, pointing to a potentially
122 beneficial role of excessive trabeculation in adults [19]. Given the diversity of underlying
123 pathophysiological mechanisms, there is ongoing debate about the significance of hypertrabeculation
124 and non-compaction within the spectrum of myocardial adaptive processes and diseases [18, 20-22].

125 Trabecular development requires the intercellular signaling action of the membrane
126 glycoprotein Neuregulin-1 (Nrg1) [4, 23-25]. This endocardial protein directly binds to epidermal growth
127 factor receptor tyrosine kinase (ErbB4) on adjacent cardiomyocytes, triggering ErbB2 ligand-
128 stimulated heterodimerization and tyrosine phosphorylation, followed by activation of downstream
129 pathways [26], including the phospho-extracellular signal-regulated kinase (pErk) intracellular signaling
130 pathway [27]. Targeted mutation of *Erbb2* or *nrg2a* in fish [3, 4, 25], or deletion of *Nrg1*, *ErbB2*, or *ErbB4*
131 in mice [24, 28-32], blocks trabeculation. Cardiomyocyte proliferation and contractility, which are
132 required for trabeculation, are impaired in mutant *ErbB4* mice [33] and *erbb2* zebrafish [3], whereas
133 potentiation of ErbB2 signaling in mouse adult cardiomyocytes promotes proliferation and myocardial
134 regeneration [34]. Consistent with these findings, beneficial effects of Nrg1 for cardiac function have

135 been reported in mouse models of cardiac injury [33]; explanted human tissue [35]; ischemic, dilated, and
136 viral cardiomyopathy [36]; and heart failure [37-39]. Clinical trials with different forms of recombinant
137 Nrg1 support a cardioprotective role in systolic heart failure [40], although the target cell-type-specific
138 effects remain to be characterized.

139 The essential role of Nrg1 in the initiation of trabeculation is well documented, but its role in
140 the cellular and molecular basis of trabecular growth, maturation, and resolution remains uncertain. In
141 particular, understanding is limited about how morphological transitions occur and progress to yield a
142 thick ventricular wall. Mutations affecting trabeculation in mice invariably lead to fetal demise [41],
143 precluding direct analysis of the mechanism(s) of trabecular growth and maturation.

144 Here, we used conditional and temporally regulated cardiac loss- and gain- of function mutants
145 and gene profiling to show that pErk activation by Nrg1 promotes trabeculation by sustaining a
146 transcriptional program regulating cell polarity, mitotic spindle orientation and cytoskeletal dynamics
147 thereby facilitating trabecular growth and maturation. Additionally, Nrg1-induced pErk activation
148 drives dynamic changes in cardiomyocyte shape and movement, leading to trabecular expansion and
149 thickening of the ventricular wall. Furthermore, this signaling cascade plays a role in timely
150 progression through the cell cycle. Notably, we identified significant overlap between Nrg1-dependent
151 genes and conserved gene signatures regulated by the ErbB2 receptor and the core component of the
152 MuvB-complex, Lin9. Both of these factors act upstream or in conjunction with the Hippo pathway,
153 which involves yes-associated protein-1 (Yap1). These findings suggest a complex interplay between
154 Nrg1-ErbB2/4-Erk and Hippo-Yap1 signaling, which holds promise for potential cardiac regeneration
155 therapies in the future.
156

157 **METHODS**
158
159 Full *Methods* are provided in the *Online Data Supplement*. Animal studies were approved by the
160 CNIC Animal Experimentation Ethics Committee and by the Community of Madrid (Ref.
161 PROEX 155.7/20). All animal procedures conformed to EU Directive 2010/63EU and
162 Recommendation 2007/526/EC regarding the protection of animals used for experimental and
163 other scientific purposes, enacted in Spanish law under Real Decreto 1201/2005.
164
165 **RESULTS**
166 **Nrg1-ErbB2/4-pErk signaling is required for trabeculae formation and expansion**
167 To study the role of Nrg1-ErbB2/4 signaling in cardiac development, we used a conditional
168 *Nrg1*^{flox} mouse line [42] (see *Methods*). We crossed *Nrg1*^{flox} mice with the *Tie2*^{Cre} driver line [43] to
169 conditionally inactivate *Nrg1* signaling in endothelial and endocardial cells from E7.5 onwards. At
170 E8.5, there were no overt differences between control and *Nrg1*^{flox};*Tie2*^{Cre} embryos, both featuring a
171 bilayered myocardial epithelium (Figure S1A,C). At E9.5, control hearts already showed nascent
172 trabeculae and a double-layered compact wall (Figure 1A; Figure S1B). In contrast, *Nrg1*^{flox};*Tie2*^{Cre}
173 mutants contained only a few trabecular projections, and the ventricular wall appeared somewhat
174 thicker (Figure 1B,C; Figure S1D). By E10.5, the trabecular network in control ventricles had become
175 more complex, whereas *Nrg1*^{flox};*Tie2*^{Cre} mutants had only a few thick, rudimentary trabeculae and a
176 noticeably thicker compact myocardium, especially in the left ventricle (Figure S1E,F,G,H).
177 *Nrg1*^{flox};*Tie2*^{Cre} mutants die by E11.5-12.5 (Suppl. Table S1, sheet 1). The profound differences in
178 compact wall thickness and trabecular network size and complexity were also revealed by 3D-
179 reconstructions (Figure 1D,E,F; Figure S1I,J; Movies S1 and S2). This defective trabecular phenotype
180 was broadly reproduced in *Nrg1*^{flox} mice crossed with the cardiac mesoderm driver line *Mesp1*^{Cre} [44]
181 (Figure S2A-D; Suppl. Table S1, sheet 2).
182 E9.5 *Nrg1*^{flox};*Tie2*^{Cre} mutant hearts showed severely attenuated endocardial Nrg1 expression
183 (Figure 1G,H). This was reflected in reduced Nrg1 signaling activity in the trabecular myocardium at
184 E9.5, indicated by weak myocardial expression of phosphorylated ErbB2 (pErbB2) (Figure 1I,J) and
185 of the phosphorylated intracellular effector Erk (pErk) (Figure 1K,L,M).
186 We examined *Nrg1* transcription at key developmental stages by *in situ* hybridization (ISH)
187 (Figure S2E-I). At E10.5 *Nrg1* was transcribed robustly and uniformly in the endocardium (Figure
188 S2E), and by E12.5 and until E16.5 at least, Nrg1 transcripts persisted in scattered cells throughout the
189 endocardium (Figure S2F-I). We further assessed pErk expression at key cardiac developmental stages
190 as a readout of Nrg1-pErbB2 activity [27, 34, 45] (Figure S2J-N). At E9.5, intense but patchy pErk signals
191 were detected in the myocardium, especially at the tips of trabeculae, but not in endocardium (Figure
192 S2J). At E11.5, pErk expression was maintained along the trabeculae, especially at the tips (Figure
193 S2K). At E12.5, strong pErk expression was found at the base of trabeculae (Figure S2L), suggesting

194 a role in the formation of endocardium-derived coronary vessels. At E13.5, weak pErk expression was
195 detected in a few myocardial cells, and stronger expression in the nascent coronaries (Figure S2M). At
196 E16.5, pErk expression was almost exclusively limited to the coronary endothelium (Figure S2N). The
197 pErk temporal expression data are consistent with a function of Nrg1 in trabecular myocardium
198 between E9.5 and E12.5, and in coronary endothelium from E13.5 onwards.
199
200 **Nrg1 is required for cardiac development patterning and proliferation**
201 To understand the basis of the defective trabeculation in *Nrg1*^{flox};*Tie2*^{Cre} mutants, we examined the
202 extracellular matrix (ECM) between endocardium and myocardium (the cardiac jelly), which is
203 required for directional migration and the formation of cardiac trabeculae [28, 46]. In control and
204 *Nrg1*^{flox};*Tie2*^{Cre} hearts at E8.5, Alcian blue staining revealed the glycosaminoglycan constituent of the
205 cardiac jelly (Figure S3A,C). However, at E9.5 and more obviously at E10.5, Alcian blue-staining was
206 severely diminished in *Nrg1*^{flox};*Tie2*^{Cre} hearts compared with controls (Figure S3B,D,E,F), consistent
207 with the manifestation of the trabeculation defect.
208 We next conducted an RNA sequencing (RNA-seq) analysis of E9.5 control and
209 *Nrg1*^{flox};*Tie2*^{Cre} hearts. We found 1,219 differentially expressed genes (DEGs; 651 upregulated and
210 515 downregulated; $P<0.05$; Table S2, sheets 1 and 2). *Nrg1*^{flox};*Tie2*^{Cre} heart sections showed severely
211 depleted expression of *Nrg1* and several key cardiac developmental genes, including the trabecular
212 marker genes *Bmp10, Hand1, Irx3,* and *Sema3a* (Figure 1N; Figure S3G). Also decreased in
213 *Nrg1*^{flox};*Tie2*^{Cre} mutants was the expression of *Has2*, which participates in the synthesis of the cardiac
214 jelly [46] (Figure 1N). ISH showed that *Has2* was restricted to a few cells in the rudimentary trabeculae
215 of *Nrg1*^{flox};*Tie2*^{Cre} mutants (Figure S3G,H), as was the expression of *Bmp10*, *Hand1, Irx3,* and *Sema3a*
216 (Figure 1O; Figure S3I-L). In further agreement, *Nrg1*^{flox};*Tie2*^{Cre} mutants had markedly depleted
217 expression of integrin alpha 6 (ITGα6) (Figure S3M-O), a trabeculae-restricted integrin [47]. In contrast,
218 ISH revealed increased *Hey2* expression in the thicker compact myocardium of *Nrg1*^{flox};*Tie2*^{Cre}
219 mutants (Figure 1O). These results indicate that abrogation of Nrg1-ErbB2/4 signaling disrupts
220 trabeculae formation and chamber myocardium patterning.
221 To define mechanisms, we performed a GSEA of "HALLMARK" gene sets [48]. Most pathways
222 were enriched (FDR q-val <0.05), including cellular stress pathways (HYPOXIA and
223 REACTIVE_OXYGEN_SPECIES_PATHWAY), associated with activation of the p53
224 (P53_PATHWAY; Figure S4A). The p53 protein responds to stresses that disrupt the fidelity of DNA
225 replication and cell division and initiates a program of cell cycle arrest, cellular senescence, or
226 apoptosis [49]. Hence, the genes contributing most to the enrichment score (the leading-edge genes) of
227 the P53_PATHWAY were associated with the cell cycle, DNA damage response, apoptosis, and other
228 processes typical of the p53 response (Figure S4A). Other enriched pathways were associated with
229 proliferation and growth (ESTROGEN_RESPONSE_EARLY, MYC_TARGETS_V2,

230 MTORC1_SIGNALING, E2F_TARGETS) (Figure 1P; Table S2, sheet 3). E2F_TARGETS represent
231 genes involved in the cell cycle, chromatin homeostasis, DNA repair, DNA replication, mitosis, and
232 other processes, including cytoskeletal regulation (Figure S4B).

233 To define the nature of the proliferative defect in *Nrg1*^{flox};*Tie2*^{Cre} hearts, we measured the
234 incorporation of bromodeoxyuridine (BrdU, an S-phase marker) from E8.5 and E10.5 (Figure 1Q;
235 Figure S5). At E8.5, the proliferation rate in mutant hearts was similar to that of control hearts (Figure
236 S5A,B). At E9.5, a statistically significant 10% relative reduction in proliferation was detected in the
237 compact myocardium of *Nrg1*^{flox};*Tie2*^{Cre} hearts (50% vs. 40%; Figure S5C-E). At E10.5, this difference
238 persisted in compact myocardium (Figure 1Q,S), whereas proliferation in the endocardium and
239 trabecular myocardium was unchanged (Figure 1Q,S). Closer inspection of the E2F_TARGET
240 "leading edge" genes further revealed that many cell cycle inhibitors including p21/*Cdkn1a,* p27/
241 *Cdkn1b,* p18/*Cdkn2c,* CIP2/*Cdkn3,* and were upregulated (Figure S4). *Cdkn1b* encodes for cyclin-
242 dependent kinase inhibitor p27^{Kip1} protein which binds and blocks cyclin-CDK to arrest the cell cycle
243 [50] and organismal growth [51, 52]. Consistent with reduced BrdU measurements, p27 protein expression
244 was readily increased in *Nrg1*^{flox};*Tie2*^{Cre} compact myocardium, but did not change in trabecular
245 myocardium (Figure 1R,T).

246 *Nrg1*^{flox};*Tie2*^{Cre} hearts were also characterized by altered pathways previously linked to
247 trabeculation in zebrafish [1, 5, 53]; namely, KRAS_SIGNALING_UP, APICAL_SURFACE, EMT
248 (EPITHELIAL_MESENCHYMAL_TRANSITION) (Figure 1P; Figure S4C,D; Table S2, sheet 3).
249 These processes, involving the cytoskeleton, cellular motility and the ECM tended to be depleted
250 although this change was only evoked (FDR qval<0.5). (Figure1P, Figure S4C,D). We surmise that
251 cardiomyocytes that typically contribute to trabeculae formation through migratory processes, remain
252 in the compact layer of *Nrg1*^{flox};*Tie2*^{Cre} mutants, leading to abnormal ventricular thickening at E9.5-
253 10.5, despite the attenuated proliferation. Overall, our data indicate that Nrg1-ErbB2/4 signaling is
254 required for both the patterning and emergence of trabeculae, and the proliferation of compact layer
255 cardiomyocytes.

256

257 **Nrg1 is required for polarity gene expression and cytoskeletal organization during trabeculation**

258 We further inspected the RNA-seq data for changes in genes associated with cell polarity and
259 cytoskeletal dynamics (Figure 2A), given they are highly interconnected developmental processes [54],
260 associated with loss of trabeculation in mice and zebrafish [1, 55, 56]. Accordingly, key genes required
261 for cytoskeletal actin remodeling (*Arf4, Dock2, Sh3bp1, Arf6*), cytoskeletal organization (*Rac1, Rac2*),
262 cell polarity (*Amotl1, Pard3, Nek3, Dlg1, Sipa1l3, Stk11, Wnt11*), cell division orientation (*Sapcd2*),
263 motility (*Kif26b, Actr2*), and Fgf-ERK signaling (*Spry2, Fgf10*) were deregulated in *Nrg1*^{flox};*Tie2*^{Cre}
264 hearts (Figure 2A).

265 The altered expression of actin remodeling genes in *Nrg1*^{flox};*Tie2*^{Cre} mutants suggested the
266 possibility of disrupted cardiomyocyte actin cytoarchitecture. Phalloidin staining of filamentous-actin
267 (F-actin) in E8.5 control embryos revealed a uniform circumferential distribution of actin filaments
268 attached to the plasma membrane (Figure 2B,C, Movies S3,S5). In contrast, in *Nrg1*^{flox};*Tie2*^{Cre} hearts
269 F-actin was non-uniformly distributed and appeared to concentrate in focal points at cell-cell junctions
270 (Figure 2B,C, Movies S4,S6), suggesting that Nrg1 is required for proper arrangement of the actin
271 cortical network. Consistent with this actin cytoskeletal defect, *Nrg1*^{flox};*Tie2*^{Cre} mutants showed
272 aberrant differential expression of genes sets for "Cytoskeleton" (GO:0005856) and "Regulation of
273 actin polymerization" (GO: 0008064)(Figure S6A,B).
274 *Nrg1*^{flox};*Tie2*^{Cre} hearts showed reduced transcription of the key cell polarity regulator *Pard3*
275 (Figure 2A, Table S2, sheet 2). *Pard3* inactivation leads to impaired apico-basal (A-B) polarity in
276 epithelial cells [57] and planar polarity defects in endothelial cells [58]. "En face" examination of
277 immunofluorescence (IF) staining in E8.5 control hearts revealed evenly distributed Pard3 protein at
278 the apical/abluminal pole of ventricular cardiomyocytes (Figure 2D left, E). In contrast, in
279 *Nrg1*^{flox};*Tie2*^{Cre} hearts, Pard3 expression was strongly reduced (Figure 2D right, E). IF in heart sections
280 confirmed Pard3 apical/abluminal pole localization in control ventricular cardiomyocytes at E8.5
281 (Figure 2F), a distribution that was maintained at E9.5 in the compact layer, whereas trabecular
282 cardiomyocytes did not express Pard3 (Figure S7A,C,C'). This observation fits with the previous
283 observations of loss of A-B polarity in cardiomyocytes that incorporate into nascent trabeculae [1]. In
284 contrast, Pard3 staining was severely depleted in E8.5 and E9.5 *Nrg1*^{flox};*Tie2*^{Cre} ventricles (Figure 2F;
285 Figure S7B,D,D'), potentially affecting A-B polarity of mutant cardiomyocytes. A second polarity
286 complex, Crumbs2, has been shown to be required for the establishment of cardiomyocyte A-B
287 polarity in zebrafish [59]. We readily detected Crumbs2 at the apical pole of the compact layer in E8.5
288 control cardiomyocytes (Figure S7E,F), but this expression was strongly depleted in *Nrg1*^{flox};*Tie2*^{Cre}
289 mutants (Figure S7G,H), consistent with a potential loss of polarity in *Nrg1*^{flox};*Tie2*^{Cre} cardiomyocytes.
290 These data indicate that loss of Nrg1 signaling is associated with depleted expression of cell polarity
291 proteins and a disorganized actin cytoskeletal network.
292
293 **Nrg1 is required for oriented division during trabeculation**
294 Dynamic interplay between polarity complexes and the cytoskeleton dictates both the positioning of
295 the mitotic spindle during mitosis and the orientation of cell division [60]. Accordingly, several genes
296 implicated in the regulation of mitotic spindle assembly were aberrantly expressed in *Nrg1*^{flox};*Tie2*^{Cre}
297 mutants, including *Cep250*, *Aurka*, *Katnb1*, *Dlg1*, *Tubgcp2*, *Kif1b* and *Kif5b*, among others (Figure
298 2G). Moreover, spindle orientation during trabeculation has been linked to the function and cellular
299 distribution of adhesion complexes [55]. The potential alteration in cell-cell adhesion molecules was
300 manifested by differential regulation of "Cell adhesion" (GO: GO:0007155) and "Regulation of cell-

301 matrix adhesion" (GO: 0001952) gene sets (Figure S6C,D). Overall, these data support the requirement
302 for Nrg1-ErbB2-pERK signaling in the transcriptional regulation of cell polarity, adhesion and spindle
303 orientation during trabeculation[55].

304 Studies in mice show that ventricular cardiomyocytes divide obliquely or perpendicular to the
305 lumen to give rise to the nascent trabeculae, whereas those that divide in parallel contribute to the outer
306 compact myocardium [6, 56] (Figure 2H). We performed IF staining against Survivin to visualize the
307 mitotic cleavage furrow and division axis during telophase (Figure 2I,J; Figure S7I-O). In E8.5 control
308 hearts, 46.2% of mitotic cardiomyocyte divisions were parallel (between 0-20º) to the ventricular
309 lumen (Figure 2I,i,J), whereas 26.9% were oblique (between 20-70º) with respect to the lumen (Figure
310 2I,J), and 26.9% perpendicular (between 70-90º; (Figure 2I,J). In contrast, in somite-matched E8.5
311 *Nrg1*^{flox};*Tie2*^{Cre} mutants, parallel divisions were significantly more frequent (76.7%; Figure 2I,ii,J) and
312 strong reductions were observed in oblique divisions (16.7%; Figure 2J,L) and perpendicular divisions
313 (6.7%; Figure 2J,M,N). In E9.5 control embryos, parallel divisions remained predominant (61.4%)
314 compared with perpendicular divisions (14%) or oblique divisions (24.6%; Figure S7I,K,M,O). In E9.5
315 *Nrg1*^{flox};*Tie2-CRE* mutants, up to 83.6% of divisions were parallel and 14.5% were oblique (Figure
316 S7J,L,O), with perpendicular divisions significantly reduced to 1.8% (Figure S7N,O). Cardiomyocyte
317 OCD is thus disrupted in E8.5-E9.5 *Nrg1*^{flox};*Tie2*^{Cre} hearts, with parallel cardiomyocyte divisions
318 favored at the expense of perpendicular divisions. We speculate that biased parallel division in
319 *Nrg1*^{flox};*Tie2*^{Cre} mutants could offset the observed reduction of proliferation at E9.5 and lead to
320 increased compact myocardium thickness.

321 **Nrg1 is required for ventricular wall formation but not coronary vessels development**

322 *Nrg1*^{flox};*Tie2*^{Cre} embryos died between E11.5-E12.5 (Table S1, sheet 1), precluding analysis of late
323 trabecular morphogenesis. To bypass this lethality, we bred *Nrg1*^{flox} and *Cdh5*^{CreERT2} mice [61] to obtain
324 mice with inducible pan-endothelial *Nrg1* deletion. Trabecular and compact wall growth was
325 drastically hindered in E13.5 *Nrg1*^{flox};*Cdh5*^{CreERT2} mice after consecutive 4-Hydroxytamoxifen (4-
326 OHT) administration at E10.5 and E11.5 (Figure S8A,B). At E16.5, this phenotype manifested as
327 thinner rudimentary trabeculae and a significantly reduced ventricular wall thickness (Figure 3A-C).
328 ISH analysis of early cardiac conduction system marker *Gja5*, the trabecular marker *Bmp10* and the
329 compact myocardium marker *Hey2* revealed loss of trabeculae patterning and expansion of compact
330 myocardium in *Nrg1*^{flox};*Cdh5*^{CreERT2} mutants (Figure 3D; Figure S8C-F). *Nrg1*^{flox};*Cdh5*^{CreERT2} mice
331 survived until E18.5 (Table S1, sheet 3). Later 4-OHT induction, at E12.5 and E13.5, did not result in
332 any obvious structural ventricular abnormalities at E18.5 (Figure S8G-K), suggesting that Nrg1–pErk
333 signaling requirement precedes E13.5.

334 To determine the molecular basis of this phenotype, we performed an RNA-seq analysis on
335 E15.5 control and *Nrg1*^{flox};*Cdh5*^{CreERT2} hearts (Table S3, sheet 1). Differential expression analysis

336 identified 44 upregulated and 31 downregulated genes (B-H p-value<0.05) (Table S3, sheet 2).
337 Differentially expressed genes were associated with pro-angiogenic and migratory processes (*Cxcr4,*
338 *Vegfb*, *Aplnr1*, *Edn1, Ednrb*, and *Angpt1* [62-65]; Figure 3E) and the development of the ventricular
339 conduction system (VCS; *Sema3a*, *Efna1, Nkx2-5, Etv1,* and *Ache* [66-70]; Figure 3E). Given that the
340 endocardium gives rise to the ventricular inner wall vessels [12, 14, 71] and that trabeculae differentiate
341 into the cardiac Purkinje Fiber network [10], these data raise the possibility that loss of endothelial Nrg1
342 expression from E11.5 onwards impairs the development of both the coronary arteries and the VCS.

343 In mice, the coronary arteries are located deep within the myocardial wall, whereas the veins
344 are located superficially, beneath the epicardial layer [72]. To assess the status of coronary vessel
345 development in *Nrg1*^{flox}*;Cdh5*^{CreERT2} mutants, we visualized the coronary network by whole-mount IF
346 for IB4 (Figure S9). This analysis revealed that the organization and complexity of the coronary arterial
347 tree was not obviously affected in E16.5 *Nrg1*^{flox}*;Cdh5*^{CreERT2} mutant hearts (Figure S9A,B,D).
348 Likewise, IF analysis of the venous endothelial marker Endomucin also revealed no appreciable
349 disturbance of venous tree organization in *Nrg1*^{flox}*;Cdh5*^{CreERT2} hearts (Figure S9E,F,H). Similar results
350 were obtained with the vascular endothelial (but not endocardial)-specific *Pdgfb*^{iCreERT2} Cre driver line
351 ([73]; Figure S9C,D,G,H).

352 We next examined the expression of classical makers of the coronary veins (*CoupTFII*),
353 arteries (*Dll4*), coronaries (*Fapbp4*), and endothelium (*Cdh5*) in developing heart by ISH, but again,
354 did not find any obvious differences in the expression nor the distribution of these specific markers
355 between E16.5 *Nrg1*^{flox}*;Cdh5*^{CreERT2} mutants and control littermates (Figure S9I-P). To quantify the
356 relative number of endothelial cells in the compact myocardium of E16.5 hearts we measured the
357 percentage of IsolectinB4-positive (IB4 +) signal in the compact myocardium (Figure S10A-C). Again,
358 there were no differences between *Nrg1*^{flox}*;Cdh5*^{CreERT2} and control hearts (Figure S10C), consistent
359 with absence of coronary vascular defect in Nrg1 mutants. Finally, we used SM22 and Notch3
360 immunostainings to determine the extent of coronary vessel smooth muscle cell differentiation and
361 pericyte coverage, respectively [72]. Consistent with the absence of coronary defects, these parameters
362 were also comparable between *Nrg1*^{flox}*;Cdh5*^{CreERT2} and control hearts (Figure S10D,E).

363 These data indicate that lack of an inner compact wall does not appreciably impact the
364 development of the coronary tree in *Nrg1*^{flox}*;Cdh5*^{CreERT2} hearts. A reasonable interpretation is that
365 the potential below-normal endocardial contribution to coronary vasculogenesis in these mutants
366 could be balanced by compensatory mechanisms involving alternative sources of endothelial cells
367 [74].

368 **Nrg1 regulates motility and G2/M progression during ventricular wall growth**

369 To identify mechanisms underlying the *Nrg1*^{flox}*;Cdh5*^{CreERT2} phenotype, we performed GSEA. Among
370 the "HALLMARK" gene sets, the most depleted pathway was EMT (-log(FDR) p-value < 0.05; Figure
371 3F; Table S3, sheet 3). The subset of leading-edge depleted genes was associated with cell

372 cytoskeleton, ECM composition, modifiers of the ECM, and transmembrane and secreted proteins
373 including adhesion molecules (Figure S11A,B). Other depleted gene sets evoked cell shape and
374 polarity, (APICAL_SURFACE, APICAL_JUNCTION), and relevant pro-migratory signaling
375 pathways, (WNT_BETA_CATENIN_SIGNALING, HEDGEHOG_SIGNALING) (Figure 3F).
376 Furthermore, depleted CHOLESTEROL_HOMEOSTASIS was consistent with the essential role of
377 Nrg1-ErbB4 signaling in cholesterol metabolism [75]. In contrast, several over-represented pathways
378 (G2/M_CHECKPOINT, E2F_TARGETS) suggested a proliferative defect (Figure 3F). The "leading-
379 edge" genes associated with these pathways were linked to the cell cycle, chromatin, DNA damage
380 response, DNA repair, DNA replication, and mitosis (Figure S11C), whereas nuclear transport,
381 transcription regulation pathways and, importantly, the cytoskeleton (Figure S11B,C), emphasize the
382 nucleus-cytoskeleton connection.

383 To support this finding, we examined E16.5 *Nrg1*^{flox}*;Cdh5*^{CreERT2} mutants for possible
384 alterations to the G1/S and G2/M cell-cycle phases by respectively measuring BrdU incorporation and
385 positivity for the early mitosis marker phospho-histone H3 (pHH3) in cardiomyocytes. Compared with
386 stage-matched control hearts, E16.5 *Nrg1*^{flox}*;Cdh5*^{CreERT2} hearts contained a significantly higher
387 proportion of pHH3-positive (pHH3+) cells, especially in trabeculae (Figure 3G,H). These differences
388 were already manifest at E12.5 (Figure S12A,B,R). There was no alteration in the proportion of BrdU+
389 cells in compact or trabecular myocardium, either at E13.5 (Figure S12C,D,G) or at E16.5 (Figure
390 S12E,F,G). The absence of effect of Nrg1 depletion on proliferation at either E12.5 or E16.5 was
391 confirmed by staining against Ki67 antigen, which preferentially marks the S-G2 phases (Figure S12H-
392 K,R). These data suggest that cell-cycle progression through the G2/M phase is delayed or prolonged
393 in *Nrg1* mutants, while the G1/S phase is unaffected.

394 To further characterize cardiomyocyte growth retardation in the *Nrg1*^{flox}*;Cdh5*^{CreERT2} mutants,
395 we examined p27^{Kip1} protein expression, as both an effector of pERK [76] and a regulator of cell cycle
396 progression at both G1/S [77] and G2/M [78] phases. p27 expression was readily increased in
397 *Nrg1*^{flox}*;Cdh5*^{CreERT2} compact and trabecular myocardium at E12.5 (Figure S12L,M,R), correlating
398 with the increase in pHH3 and a potentially delayed G2/M phase. This difference persisted in compact
399 myocardium at E16.5, although the overall p27 staining in both control and mutant was severely
400 attenuated by this timepoint (Figure S12N-Q,R).

401 Overall, the analysis of the *Nrg1*^{flox}*;Cdh5*^{CreERT2} transcriptome suggests that Nrg1 regulates
402 trabecular growth and chamber wall formation by coordinating cell migration and G2/M phase
403 progression.

404

405 **Ectopic Nrg1 expression induces trabeculation of ventricular wall myocardium**

406 To gain further insight into the role of Nrg1 in chamber development, we created a conditional Nrg1
407 gain-of-function model. For this, we generated a transgenic line bearing a *Rosa26-floxNeoSTOPflox-*

408 *Nrg1-EGFP* expression cassette (Figure S13A,B; see *METHODS*). Nkx2-5^{Cre}-mediated removal of the
409 NeoSTOP sequence resulted in the expression of both the GFP reporter (Figure S13C,D) and Nrg1
410 protein (Figure S13E,F). Examination of E16.5 embryos showed that *R26Nrg1^{GOF};Nkx2-5^{Cre}*
411 transgenic hearts were developmentally arrested, with an appearance similar to that of E12.5 wild-type
412 hearts (Figure S14A,B). This developmental arrest was further evidenced by the presence of a double-
413 outlet right ventricle, leading to overriding aorta (Figure S14A) and a ventricular septal defect
414 (muscular and peri-membranous; Figure S14B). E16.5 *R26Nrg1^{GOF};Nkx2-5^{Cre}* transgenic hearts also
415 displayed superficial outgrowths resembling fistulae (Figure S14Ci,ii), which were possibly
416 manifestations of direct communication between the endocardium and epicardium caused by
417 considerable thinning of the compact myocardium (Figure 3I,L). *R26Nrg1^{GOF};Nkx2-5^{Cre}* mice die by
418 E18.5 (Table S1, sheet 4).

419 Histological analysis of E16.5 hearts showed that the transgenic epicardium consisted of 3–4
420 cell layers instead of a single cell layer (Figure S14D), and the sub-epicardial layer was extensively
421 infiltrated by endothelial cells but largely devoid of coherent large vessel conduits (Figure 3I; Figure
422 S14D). Cardiomyocyte morphology (roundness) in the outer compact myocardium of
423 *R26Nrg1^{GOF};Nkx2-5^{Cre}* transgenic hearts resembled more the trabecular myocardium of controls than
424 the corresponding compact myocardium (Figure 3J,K,M). Moreover, expression of ITGα6 was
425 expanded in E10.5 *R26Nrg1^{GOF};Nkx2-5^{Cre}* hearts from the trabeculae to the compact layer (Figure
426 S14E,F). Thus, Nrg1 overexpression causes the compact myocardium to become trabecular-like.

427 To define the molecular underpinnings of this phenotype and to compare with the one obtained
428 from *Nrg1^{flox};Cdh5^{CreERT2}* hearts, we performed RNA-seq on E15.5 transgenic hearts. Differential
429 expression analysis identified > 4,500 DEGs in *R26Nrg1^{GOF};Nkx2-5^{Cre}* hearts (FDR q-value<0.05;
430 Table S4, sheets 1 and 2). As expected, the expression of a subset of His-Purkinje-specific genes [79]
431 was broadly upregulated (Figure 3N). ISH analysis revealed expansion of *Gja5* transcription towards
432 the compact myocardium (Figure 3O), consistent with the proposed role of Nrg1 as a driver of VCS
433 specification and differentiation [80]. Pathway analysis revealed the enrichment for pro-migratory
434 processes (EMT, APICAL_JUNCTION, KRAS_SIGNALING_UP) in *R26Nrg1^{GOF};Nkx2-5^{Cre}* hearts
435 (Figure 3P), involving expression of the EMT transcription factor drivers Snail and Twist genes
436 (Figure S15A; Table S4, sheets 2 and 3), as well as several key EMT signaling pathways, including
437 TGFβ (TGF_BETA_SIGNALING) and BMP (Figure 3P; Figure S15B,C; Table S4, sheets 2 and 3).

438 Conversely, metabolic pathways (ie.: OXIDATIVE_PHOSPHORYLATION,
439 FATTY_ACID_METABOLISM, ADIPOGENESIS, PROTEIN_SECRETION, MYOGENESIS,
440 CHOLESTEROL_HOMEOSTASIS), associated with MYC activity (MYC_TARGET_V1,
441 MYC_TARGET_V2) (Figure 3P, Table S4, sheets 2 and 3), were depleted, revealing an impairment
442 of cardiac metabolic maturation. In support of this maturational defect, we examined the expression
443 of intermediate filament genes as they have been involved in lineage determination and organ

444 maturation [81]. Several genes encoding lamins, nestin and various keratin proteins were differentially
445 regulated in *R26Nrg1*^{GOF}*;Nkx2-5*^{Cre} hearts (Figure S15D). Notably, mis-expression of the intermediate
446 filament protein Nestin, has been characterized as a marker of cardiac immaturity [82]. Thus, in E16.5
447 control hearts, Nestin expression was weak in trabecular myocardium but strong in endothelium and
448 epicardium (Figure S14Gi,i'). In contrast, in *R26Nrg1*^{GOF}*;Nkx2-5*^{Cre} transgenic hearts, Nestin
449 expression was substantial in the trabecular layer and expanded sub-epicardium layer, devoid of α-
450 smooth-muscle actin (SMA) staining (Figure S14Hii,ii′). Overall, Nrg1 overexpression alters the
451 relative proportion of constituent ventricular wall cell types and causes the compact myocardium to
452 become trabecular-like
453
454 **Ectopic Nrg1 expression causes cell cycle arrest and a pro-senescence phenotype**
455 The metabolic defect was also associated with the upregulation of cytotoxic stress
456 (IL6_JAK_STAT3_SIGNALING, HYPOXIA, IL2_STAT5_SIGNALING, UNFOLDED PROTEIN
457 RESPONSE), pro-inflammatory (INFLAMMATORY_RESPONSE, COAGULATION,
458 COMPLEMENT, ALLOGRAFT_REJECTION, INTERFERON_GAMMA_RESPONSE), and pro-
459 senescence (TNA_SIGNALING_VIA_NFKB) gene sets (Figure 3P; Figure S15E,F; Table S4, sheet
460 3). The activation of cellular stress pathways suppresses mitogenic responses and promotes senescence
461 [83], and have been previously associated with the so-called "hypermitotic" cell cycle arrest
462 phenomenon [84].
463 Indeed, the depletion of cell-cycle–related gene sets (E2F_TARGETS and
464 G2M_CHECKPOINT) (Figure 3P), suggested a proliferation defect associated with the fetal
465 developmental arrest of *R26Nrg1*^{GOF}*;Nkx2-5*^{Cre} embryos. We examined E12.5 and E16.5
466 *R26Nrg1*^{GOF}*;Nkx2-5*^{Cre} mutants for possible alterations to the G1/S and G2/M cell-cycle phases. The
467 proportion of BrdU+ cells was lower in the compact and trabecular myocardium of E16.5
468 *R26Nrg1*^{GOF}*;Nkx2-5*^{Cre} hearts (Figure 3Q,R), suggesting either decreased proliferation rate, or delayed
469 G1/S progression. The inhibitory effect of Nrg1 expression on compact and trabecular cardiomyocytes
470 proliferation was confirmed by staining against Ki67 antigen (Figure S16A-D). In contrast, the pHH3+
471 cell indexes in compact myocardium were similar in E12.5 and E16.5 control and *R26Nrg1*^{GOF}*;Nkx2-*
472 *5*^{Cre} transgenic hearts (Figure S16E,F,I), although in trabecular myocardium at E12.5, pHH3+ staining
473 was increased, but no longer at E16.5 (Figure S16E,F,I). These data suggest that the proliferation rate
474 across the ventricular wall is homogeneously decreased in *R26Nrg1*^{GOF}*;Nkx2-5*^{Cre} transgenic hearts,
475 consistent with the suggested myocardial "trabeculation" of the compact layer.
476 Closer inspection of the E2F_TARGET genes revealed several key cell cycle inhibitors that
477 were either increased (*cdkn1a*/p21) or decreased (*cdkn1b*/p27, *cdkn2c*/p18) (Figure S15G), as
478 potentially underlying the growth retardation defect. We examined the expression of the p27 inhibitor
479 of cell cycle progression [85] in E12.5 *R26Nrg1*^{GOF}*;Nkx2-5*^{Cre} embryos, and found it to be markedly

480 increased in compact and trabecular myocardium compared to controls (Figure S16G,I), correlating
481 with the decrease in BrdU+ labelling (Figure 3Q,R) and a potentially delayed G1/S phase. Here,
482 *cdkn1b* gene expression did not correlate with its protein expression, likely because regulation of p27
483 is predominantly post-transcriptional [86]. This increased p27 expression persisted in compact
484 myocardium at E16.5, although the overall p27 staining in both control and mutant was severely
485 attenuated by this stage (Figure S16H,I). Overall, these data indicate that Nrg1 overexpression
486 promotes cell cycle arrest and a prosenescence phenotype.
487
488 **Nrg1 regulates ventricular patterning mediated by cytoskeletal dynamics**
489 Analysis of chamber trabecular and compact myocardium markers revealed profoundly altered
490 myocardial wall structure and patterning in both the *Nrg1*^{flox}*;Cdh5*^{CreERT2} mutant and
491 *R26Nrg1*^{GOF}*;Nkx2-5*^{Cre} transgenic hearts (Figure 4A-L). At E16.5, SMA is normally confined to the
492 immature and proliferative compact myocardium ([87]; Figure 4D) but extended along the length of
493 trabeculae in *Nrg1*^{flox}*;Cdh5*^{CreERT2} hearts (Figure 4E), consistent with defective trabecular maturation
494 and maintenance of compact myocardium identity. In contrast, SMA was markedly reduced in the
495 compact myocardium of *R26Nrg1*^{GOF}*;Nkx2-5*^{Cre} transgenic hearts (Figure 4F), in line with a loss of
496 compact myocardium identity and gain of trabecular one. In agreement with these findings, ISH
497 showed that *Hey2* expression abnormally extended into the trabeculae of *Nrg1*^{flox}*;Cdh5*^{CreERT2} hearts,
498 contrasting its normal restriction to the compact myocardium (Figure 4G,H), and was almost
499 completely absent from *R26Nrg1*^{GOF}*;Nkx2-5*^{Cre} ventricles (Figure 4G,I), reflecting loss of compact
500 myocardium identity. Conversely, *Bmp10* expression was attenuated in the trabeculae of
501 *Nrg1*^{flox}*;Cdh5*^{CreERT2} mutants (Figure 4J,K) and extended into the compact layer in *R26Nrg1*^{GOF}*;Nkx2-*
502 *5*^{Cre} transgenic embryos (Figure 4J,L), reflecting acquisition of trabecular identity. Thus, Nrg1 loss of
503 function causes trabecular myocardium to become compact-like, whereas Nrg1 gain-of-function
504 causes compact myocardium to become trabecular-like.
505 Tissue patterning is determined, in part, by the organization of cytoskeletal components [88]. In
506 cardiomyocytes, these components form the sarcomere, which are bundles of polymerized actin
507 crosslinked by α-actinin (Z-line) and arranged in a stacked striated pattern throughout muscle tissue.
508 We therefore examined changes in the actin cytoskeleton potentially underlying the patterning defects,
509 by examining F-actin (Phalloidin) and α-actinin (Figure 4M-O). In control E10.5 hearts, the intensity
510 of Phalloidin staining was markedly higher in trabecular compared to compact myocardium, in contrast
511 to α-actinin, which displayed similar intensity of staining (Figure 4M,N). Phalloidin staining in
512 trabecular myocardium was normalized to compact myocardium intensity in E10.5 *Nrg1*^{flox}*;Tie2*^{Cre}
513 mutants, while staining in compact myocardium was normalized to trabecular myocardium level in
514 E10.5 *R26Nrg1*^{GOF}*;Nkx2-5*^{Cre} hearts (Figure 4M,N). Thus, the contrast between F-actin staining
515 intensities was absent in both *Nrg1*^{flox}*;Tie2*^{Cre} and *R26Nrg1*^{GOF}*;Nkx2-5*^{Cre} hearts, which is consistent

516 with the loss of trabecular and compact myocardium identities, respectively. We investigated the
517 arrangement of cardiomyocytes by visualizing their sarcomeres using IF against α-actinin (Figure
518 4O). The sarcomeres in trabecular cardiomyocytes of E16.5 control, *Nrg1*^{flox}*;Cdh5*^{CreERT2} and
519 *R26Nrg1*^{GOF}*;Nkx2-5*^{Cre} hearts exhibited a well organized striation pattern (Figure 4Oi). In the compact
520 myocardium of control hearts, cardiomyocytes displayed two distinct fiber patterns based on their
521 striation; those in the inner compact myocardium exhibited a circular striation pattern (Figure 4Oii),
522 while cardiomyocytes in the outer compact myocardium displayed a similar fiber orientation as in the
523 trabeculae (Figure 4Oiii). Analysis of sarcomere fiber orientation revealed that *Nrg1*^{flox}*;Cdh5*^{CreERT2}
524 hearts exhibited a deficiency in the inner compact myocardium layer, while maintaining a normal outer
525 compact myocardium (Figure 4Oii, iii). Conversely, the compact myocardium of *R26Nrg1*^{GOF}*;Nkx2-*
526 *5*^{Cre} ventricles displayed a sarcomere fiber orientation akin to that of the trabecular myocardium
527 (Figure 4Oi-iii). Upon closer inspection, *Nrg1*^{flox}*;Cdh5*^{CreERT2} compact-myocardium sarcomeres
528 appeared slightly more diffuse than their control counterparts and contained ring-like structures
529 (Figure 4P,Qii,iii), suggesting disruption of Z-line alignment. The striated sarcomere structure
530 revealed by α-actinin was also broadly evident from F-actin staining, including the presence of ring-
531 like structures in *Nrg1*^{flox}*;Cdh5*^{CreERT2} hearts (Figure 4Qii,iii), suggesting mis-arrangement of F-actin
532 branching. Similar ring-like structures were detected in the compact myocardium sarcomeres of
533 *R26Nrg1*^{GOF}*;Nkx2-5*^{Cre} hearts (Figure 4Rii,iii). Overall, these data indicate that above-normal or
534 below-normal Nrg1 expression causing the ventricular patterning defects are associated with disrupted
535 F-actin organization and sarcomere Z-line positioning.
536
537 **Nrg1 modulates pErk-dependent Yap1 S274 phosphorylation during trabeculation**
538 Having identified myocardial pErk as a read-out of Nrg1 signaling during trabeculation (see Figure
539 1K-M; Figure S2J-N;), we monitored pErk expression in *R26Nrg1*^{GOF}*;Nkx2-5*^{Cre} transgenic hearts. In
540 E9.5 control hearts, pErk was expressed in trabeculae and in cardiomyocytes close to the ventricular
541 lumen (Figure 5A), and additionally in some epicardial cells at E11.5 (Figure 5C). In contrast, E9.5-
542 E11.5 *R26Nrg1*^{GOF}*;Nkx2-5*^{Cre} transgenic hearts showed ectopic pErk expression in the compact
543 myocardium and sub-epicardial layers (Figure 5B,D). From E13.5 onwards, pErk was no longer
544 detected in the myocardium of control hearts (Figure S2M,N), but was expressed in coronary
545 endothelial cells (Figure S17A), similarly to the observation in *Nrg1*^{flox}*;Cadh5*^{CreERT2} hearts (Figure
546 S17B). At E16.5, pErk was no longer expressed ectopically in *R26Nrg1*^{GOF}*;Nkx2-5*^{Cre} myocardium
547 (Figure S17C).
548 To support these findings, we examined the expression of pErbB2 and pErbB4 during
549 compaction. In E16.5 control hearts, pErbB2 and pErbB4 were both strongly expressed in coronary
550 endothelium, sparsely expressed in endocardium, and absent from myocardium (Figure S17D,G).
551 pErbB2 was also readily detected in epicardium (Figure S17D). In *Nrg1*^{flox}*;Cadh5*^{CreERT2} hearts, the
552 strong coronary endothelial expression and sparse endocardial expression were maintained (Figure

553 S17E,H). In *R26Nrg1*^{GOF}*;Nkx2-5*^{Cre} hearts, strong pErbB2 and pErbB4 expression was detected in both
554 endothelium and endocardium, and remained absent from myocardium (Figure S17F,I). Thus, during
555 compaction, pErbB2 and pErbB4 are no longer expressed in myocardium, and cannot be induced by
556 Nrg1 in this tissue.

557 We noticed that the *R26Nrg1*^{GOF}*;Nkx2-5*^{Cre} gene signature closely mirrored gene signatures
558 found in adult mouse hearts overexpressing the ErbB2 receptor (ErbB2^{OE}) [89] and in fetal hearts
559 deficient for the activator MuvB core complex component Lin9 (Lin9^{KO}) [90] (Figure S17J,K). Notably,
560 the EMT and oxidative phosphorylation gene signatures were respectively enriched and depleted in
561 the transcriptomes of all three of these models, whereas the opposite change occurred after Nrg1
562 deletion (Figure 3F, S17L). ErbB2-mediated cardiac regenerative phenotypes are mediated, in part, by
563 Yap1 [89], and there is significant overlap between the conserved Yap1-regulated and Lin9-dependent
564 gene signatures [91]. Enrichment analysis revealed that many of the differentially-regulated genes in
565 ErbB2^{OE} and Lin9^{KO} hearts were also significantly altered in the Nrg1 transcriptomes (Figure 5E,F;
566 Figure S17L). Moreover, the E15.5 *R26Nrg1*^{GOF}*;Nkx2-5*^{Cre} transcriptome displayed significant overlap
567 with the Yap1 target gene signature [92] (Figure S18A). Part of this enriched gene signature
568 corresponded to the EMT pathway (Figure S17L), suggesting that a significant portion of the Nrg1
569 transcriptome involving cytoskeletal genes might also be YAP-dependent.

570 The activation/inactivation of Yap by canonical Hippo-dependent and non-Hippo dependent
571 phosphorylations has been linked to mechano-transduction and mitosis during cardiac regeneration [89].
572 ErbB2 signaling via Erk elicits cytoskeletal changes with an altered mechanical state and downstream
573 YapS274 phosphorylation, resulting in pYap activation and nuclear localization [89]. Given the
574 enrichment of Yap1-target genes in *R26Nrg1*^{GOF}*;Nkx2-5*^{Cre} hearts, we examined the Nrg1 mutants for
575 Hippo (Mob1)-dependent Yap1 phosphorylation on S112 (S127 in human) and pErk and mitosis-
576 associated Yap1 phosphorylation on S274 (S289 in human) [93, 94]. In control E9.5 hearts, pYap S112
577 was strongly expressed in the cytoplasm of endocardial cells and weakly expressed in some
578 cardiomyocytes (Figure S18B). In *Nrg1*^{flox}*;Tie2*^{Cre} hearts, pYap S112, while maintained in
579 endocardium, was not visible in cardiomyocytes (Figure S18C). Interestingly, pMob1-Thr35
580 expression was also below normal (Figure 5I), suggesting that Hippo-dependent Yap1 nuclear
581 localization would be higher in E9.5 *Nrg1*^{flox}*;Tie2*^{Cre} hearts. However, at E13.5, pYap S112 was present
582 exclusively in endocardial cells in both control and *Nrg1*^{flox}*;Cadh5*^{CreERT2} hearts (Figure S18D,E), and
583 the same restriction was observed at E16.5 in control and *R26Nrg1*^{GOF}*;Nkx2-5*^{Cre} hearts (Figure
584 S18F,G). Thus, pYap S112 expression and Hippo-regulated Yap activity appear to be dependent on
585 Nrg1 at E9.5, but independent of Nrg at E13.5 or E16.5.

586 At E9.5, pYap S274 was localized in the nuclei of myocardial cells in control hearts (Figure
587 5G) but was mostly cytoplasmic in *Nrg1*^{flox}*;Tie2*^{Cre} hearts (Figure 5H). In agreement with this, Western

588 blot analysis revealed below-control pYap S274 expression in *Nrg1*^{flox}*;Tie2*^{Cre} hearts (Figure 5I).
589 Consistent with the dependence of pYap S274 on Erk phosphorylation [89], pErk expression was also
590 below control (Figure 1M). In contrast, at E16.5, pYap S274 IF labeled only scattered cells in the
591 myocardium of control, *Nrg1*^{flox}*;Cdh5*^{CreERT2}, and *R26Nrg1*^{GOF}*;Nkx2-5*^{Cre} hearts (Figure S18H-J),
592 although Western blot analysis detected above control-level expression of pMob1-Thr35 in both Nrg1
593 LOF and GOF mutants (Figure 5J,K). These data suggest that Erk phosphorylation, pYap S274 cellular
594 distribution and Hippo/Mob1 activity in cardiomyocytes, are dependent on Nrg1 during trabeculation
595 but not during compaction

596 **Discussion**

597 The results presented here show that Nrg1 regulates a distribution of polarized morphologies and
598 division dynamics across the ventricular wall (Figure 5L). We interpret our findings in light of a body
599 of work showing that trabeculation is a dynamic process involving transient disruption of the integrity
600 of the myocardial cell layer. In zebrafish this manifests as an EMT-like process that involves changes
601 in the actin cytoskeleton network, resulting in actomyosin polarization, apical constriction,
602 depolarization, and delamination without division [1, 3-5, 53, 95]. In mice, the realignment of the dividing
603 axis of cardiomyocytes undergoing trabeculation involves transient disruption and re-positioning of
604 polarity, focal cell and matrix adhesion complexes [6, 7, 56]. Furthermore, interlinked posttranscriptional
605 and transcriptional cascades converge to drive dynamic changes in the contractile actomyosin network,
606 influence force transmission, to control spindle orientation and directional migration [54, 60].

607 We infer from our transcriptomics data that Nrg1 regulates the expression of genes required
608 for cell shape and morphology, including key polarity complex components, with depletion of the
609 apical junction and polarity proteins Pard3 and Crumbs2, which have been linked to oriented division
610 and trabeculation [56, 59] (Figure 5L). These changes were further associated with evidence of ventricular
611 wall defects and altered expression of cell junctional components required for structural integrity of
612 the myocardium [6, 7, 55]. The disrupted actin cytoarchitecture in early Nrg1 mutants causes a failure to
613 acquire the motile and invasive behaviors required for proper orientation of the mitotic spindle and
614 orthogonal cardiomyocyte division. Later trabecular growth and elongation phases are driven by EMT-
615 like migration of cardiomyocytes derived from the growing outer compact layer towards the trabeculae
616 (Figure 5L).

617 The initial thickening of the inner myocardial wall therefore depends on the formation of a
618 mixed trabecular/compact zone closest to the source of Nrg1. The outer compact myocardium initially
619 consists of just 2-3 layers, but attains a thickness of about 15-20 cell layers by the end of trabeculation
620 (Figure 5L), likely through differential growth [96]. We surmise that the inner compact myocardium acts
621 as a "feeder" layer for trabecular growth, [6]consistent with previous analyses identifying clones of
622 migratory cells spanning anatomical transmural locations during ventricular chamber formation [6, 8,
623 95, 97, 98]. These EMT-like processes involve disruption of cell–cell interactions and disassembly of the
624 polarity complexes, with rearrangement of actin filaments to bestow invasive behaviors required for
625 cellular motility [99]. However, they take place in the absence of the activation of canonical EMT
626 transcription factors or the acquisition of mesenchymal-specific markers and do not involve the
627 establishment of a front-to-back polarity, suggesting that this type of EMT is partial or incomplete [99].
628 Thus, Nrg1 regulates the spatial distribution of compact and trabecular myocardium by generating
629 molecularly distinct myocardial layers and establishing the boundaries of trabecular identity (Figure
630 5L).

631 Consistent with this notion, by promoting the development of the trabecular and the adjacent
632 inner compact myocardium, Nrg1 restricts the growth of the proliferative cardiomyocytes of the outer
633 layer. By analogy with the situation in lung airway epithelium cell division [100], parallel cardiomyocyte
634 division may be the default orientation for myocardial growth. Nrg1-ErbB2/4-Erk1/2 signaling activity
635 may function as a switch to override this default orientation, although not by providing any orientation
636 cue, but rather by determining whether or not a cell responds to such cues. These could be provided
637 by cell polarity pathways, as they play important roles in regulating mitotic spindle angle distribution
638 in epithelial tissues [60]. We can surmise that, in addition to transcriptional regulatory mechanisms, a
639 Nrg1-pERK kinase cascade may exert effects (direct and indirect) on the centrosomal components of
640 the mitotic spindle, or the cytoskeletal elements that control centrosome position and spindle
641 orientation [101].

642 Nrg1 overexpression causes a profound change in compact ventricular wall composition,
643 increasing the proportion of endothelial and epicardial cells relative to that of cardiomyocytes. This
644 suggests that, as development advances, patterning and growth of the outer compact layer no longer
645 depends on Nrg1 [102], as cardiomyocytes are no longer sensitive to signals emanating from the
646 endocardium, and the activation of the downstream effector pErk is suppressed in the myocardium,
647 likely through downregulation of the ErbB2/4 receptors. This would be consistent with a spatio-
648 temporal range of action confined to the trabecular period of ventricular wall development.
649 Consequently, by virtue of their comparatively higher proliferation rate, compact layer cardiomyocytes
650 eventually outgrow trabecular cardiomyocytes during the compaction phase [13]. Specification to
651 trabecular versus compact myocardium may therefore depend on the relative distance of
652 cardiomyocytes from the source of Nrg1, as its influence becomes limited to the endocardium-
653 proximal cardiomyocytes giving rise to the subendocardial ventricular myocardium and Purkinje fiber
654 conduction system network [79] (Figure 5L).

655 Our studies underscore the tight coordination between cell division and migration that evolved
656 to ensure pattern and boundary formation during tissue growth and morphogenesis [103-105]. In addition
657 to the morphogenic EMT-like component, Nrg1 regulates gene signatures for cell-cycle progression
658 linked to mitosis, DNA replication and repair, and the cytoskeleton [106-108]. There is a close association
659 between cytoskeleton organization, cell adhesion, and the cell cycle [109], revealed by actin-regulated
660 G2/M checkpoint controls[110-112], and our interpretation of the mutant phenotype is plausible if Nrg1-
661 pErk signaling is required for progression through the G2/M phase. Consistent with this idea, ERBB2
662 (HER2) and ERK1/2 have been identified as important regulators of the G2/M checkpoint response to
663 genotoxic stress [113, 114]. Further, these studies highlight 2 types of cell cycle arrest [84, 115]: 1) classical
664 (hypomitogenic) growth arrest caused by growth factor withdrawal, is an exit from the cell cycle
665 characterized by the inactivation of both upstream (Ras-Mapk signaling) and downstream proliferation
666 factors (cyclins); 2) hypermitogenic cell cycle arrest caused when mitogen-activate pathways are

active but cell cycle progression is blocked downstream (for example p21/p27 over-expression), ultimately leading to a senescence-like phenotype.

With regard to Nrg1-pErk and Hippo-Yap1 interactions, available evidence indicates that: 1) Nrg1 activates endogenous ErbB4 to induce Yap1 target genes in breast cancer cells [75]; 2) ErbB2 drives mitosis during cardiac regeneration via pErk-dependent and Hippo-independent Yap1 activation [89]; 3) Interaction of Yap1 with the Myb-MuvB (MMB) complex promotes mitotic gene expression in fetal cardiomyocytes [90]; and 4) Yap1-mediated cardiac regeneration requires the transcription of cell-cycle, adherens-junction, and cytoskeletal genes [92, 116-118]. Considering this, Yap1 could act as a downstream effector of Nrg1 during trabeculation (Figure 5L) as there exists a significant overlap between Nrg1, ErbB2 and YAp1 GOF, and Lin9 inactivation gene signatures, involving EMT-like genes, and we provide evidence suggesting that Nrg1 is required for Yap1(S274) nuclear localization during early trabeculation but not during compaction, consistent with a restricted Nrg1-pErk window of function. Intriguingly, the Yap1 homolog WWTR1 promotes compact wall development by inhibiting trabeculation in zebrafish, whereas Nrg1-ErbB2 signaling negatively regulates WWTR1 nuclear localization and activity [31]. These findings provide incentives for further studies into the role of Nrg1-Yap1 in ventricular wall development.

Our studies provide evidence that non-compaction/hypertrabeculation is a defect of asymmetric ventricular wall growth. Because of the considerable overlap between trabeculation and ventricular wall maturation and compaction, it has been difficult to distinguish excessive trabeculation from the failure to compact and to determine whether these phenotypes form part of a continuum or are separate entities. Experimental evidence from human induced pluripotent cell models suggests that non-compaction might be attributable to defective cardiomyocyte proliferation [119], whereas data from mice show that the persistence of trabeculae postnatally may be the result either of excessive proliferation of trabecular cardiomyocytes [120, 121] or of reduced proliferation in compact myocardium [13, 20, 122]. Our studies help to resolve this conundrum by suggesting that non-compaction/hypertrabeculation is linked to disrupted asymmetric growth and differentiation across the ventricular wall, resulting in defective trabecular patterning and cardiomyocyte proliferation. The extensive overlap between cell division and morphogenesis makes it difficult to discern the individual contributions of these processes to trabecular and compact myocardium growth. The possibility of multi-omic measurement at single-cell scale provides an incentive for future investigation.

Acknowledgments

We thank A. Galicia and L. Méndez for mouse husbandry, the Genomics Units for carrying out RNA-seq, and S. Bartlett for English editing.

Sources of Funding

This study was supported by grants PID2019-104776RB-I00 and PID2020-120326RB-I00, CB16/11/00399 (CIBER CV) from MCIN/AEI/ 10.13039/501100011033, a grant from the Fundación BBVA (Ref.: BIO14_298), a grant from Fundació La Marató de TV3 (Ref.: 20153431) and a grant from the Spanish Society for Cardiology (SECSCFG-INV-CFG 21/004) to J.L.d.l.P. J.G-B. was funded by Programa de Atracción de Talento from Comunidad de Madrid (Ref. 2016T1/BMD1540). The cost of this publication was supported in part with funds from the European Regional Development Fund. The CNIC is supported by the ISCIII, the MCIN and the Pro CNIC Foundation and is a Severo Ochoa Center of Excellence (grant CEX2020001041-S) financed by MCIN/AEI /10.13039/501100011033.

Disclosures None.

714 **Figure Legends**

715

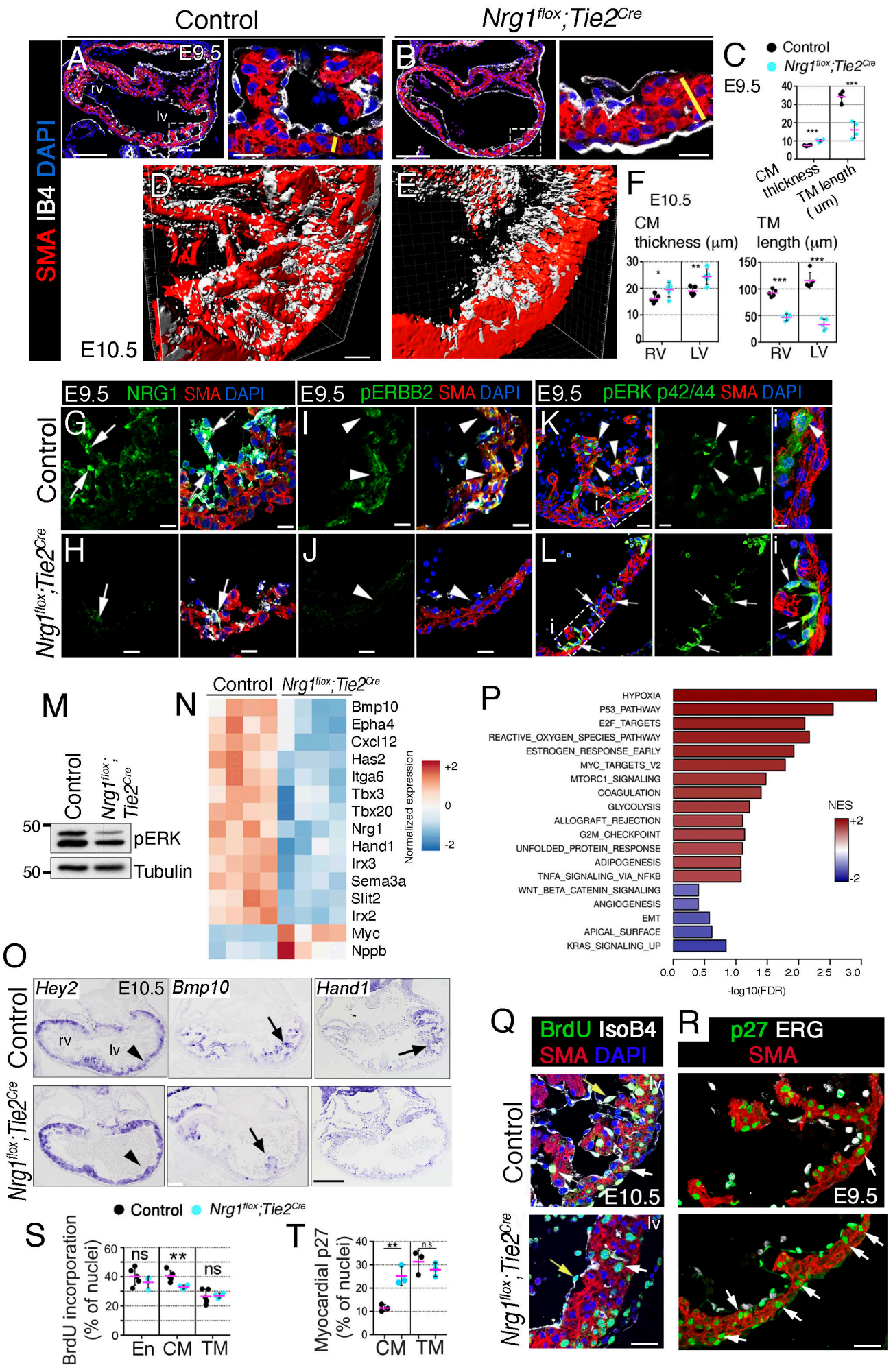

Figure 1_Grego-Bessa

716 **Figure 1. Nrg1-ErbB2-pErk signaling is required for trabeculation initiation and expansion.**
717 **(A,B)** Immunofluorescence against smooth muscle actin (SMA, red) and isolectin B4 (IB4, white) in
718 heart sections from E9.5 control **(A)** and *Nrg1*^{flox}*;Tie2*^{Cre} embryos **(B)**. Yellow lines mark the thickness
719 of the compact myocardium (CM). Sections were counterstained with DAPI (blue). **(C)** Quantification
720 of CM thickness and trabecular myocardium (TM) length in control and *Nrg1*^{flox}*;Tie2*^{Cre} left ventricles
721 at E9.5. **(D, E)** 3D reconstruction of SMA-stained E10.5 control and *Nrg1*^{flox}*;Tie2*^{Cre} left ventricles.
722 **(F)** Quantifications of CM thickness and TM length in control and *Nrg1*^{flox}*;Tie2*^{Cre} ventricles at E10.5.
723 **(G-L)** Immunofluorescence against Nrg1, pErbB2, and pErk (green) in E9.5 control embryos **(G, I,**
724 **K)** and *Nrg1*^{flox}*;Tie2*^{Cre} embryos **(H, J, L)**. SMA, red; IB4, white; DAPI counterstain, blue. Arrows
725 mark endocardium, arrowheads mark myocardium. **(M)** Representative western blot of pErk in E9.5
726 ventricles (pool of n = 3 per genotype). **(N)** Heatmap of representative differentially expressed genes
727 (DEGs) in E9.5 control vs. *Nrg1*^{flox}*;Tie2*^{Cre} hearts. The color code represents normalized gene
728 expression from -2 to +2. **(O)** ISH of *Hey2*, *Bmp10*, and *Hand1* in E9.5 control and *Nrg1*^{flox}*;Tie2*^{Cre}
729 embryos. Arrows mark TM, arrowheads CM. **(P)** Hallmark Gene Set Enrichment Analysis (GSEA)
730 for E9.5 *Nrg1*^{flox}*;Tie2*^{Cre} vs. Control. The bar plot represents enrichment data for 19 Hallmark gene
731 sets at a false discovery rate FDR qval < 0.1 and FDR qval < 0.5, for gene sets with positive or negative
732 enrichment score, respectively. Of those gene sets, 8 had an FDR qval < 0.05. The scale bar represents
733 normalized enrichment score (NES) from -2 to +2. Positive scores (red), indicating enrichment in
734 *Nrg1*^{flox}*;Tie2*^{Cre} relative to the control condition, were found for 14 gene sets, and negative scores
735 (blue), indicating depletion, were found for 5 gene sets. Relative expression values for the "leading
736 edge" genes associated to gene sets P53_PATHWAY, E2F_TARGETS, KRAS_SIGNALING_UP
737 and EMT are presented as heatmaps in Figure S4. **(Q)** BrdU immunodetection in E10.5 control and
738 *Nrg1*^{flox}*;Tie2*^{Cre} embryos. Arrows mark myocardium, arrowheads endocardium. **(R)** p27
739 immunodetection in E9.5 control and *Nrg1*^{flox}*;Tie2*^{Cre} embryos. Arrows mark myocardium. **(S)**
740 Quantification of BrdU incorporation in E10.5 control embryos (n=4) and *Nrg1*^{flox}*;Tie2*^{Cre} embryos
741 (n=3). **(T)** Quantification of p27 immunostaining in E9.5 control and *Nrg1*^{flox}*;Tie2*^{Cre} embryos (n=3
742 per genotype). En, endocardium; RV, right ventricle; LV, left ventricle. * $P < 0.05$, ** $P < 0.01$, $P <$
743 0.001; ns, non-significant by Student t-test. Scale bars, 200 μm (low magnification in A,B, and O);
744 50μm (D,E); 20 μm (high magnification in A,B and G, I, K H, J, L, Q, and R); 10 μm (high
745 magnification in Gi,Hi).

746

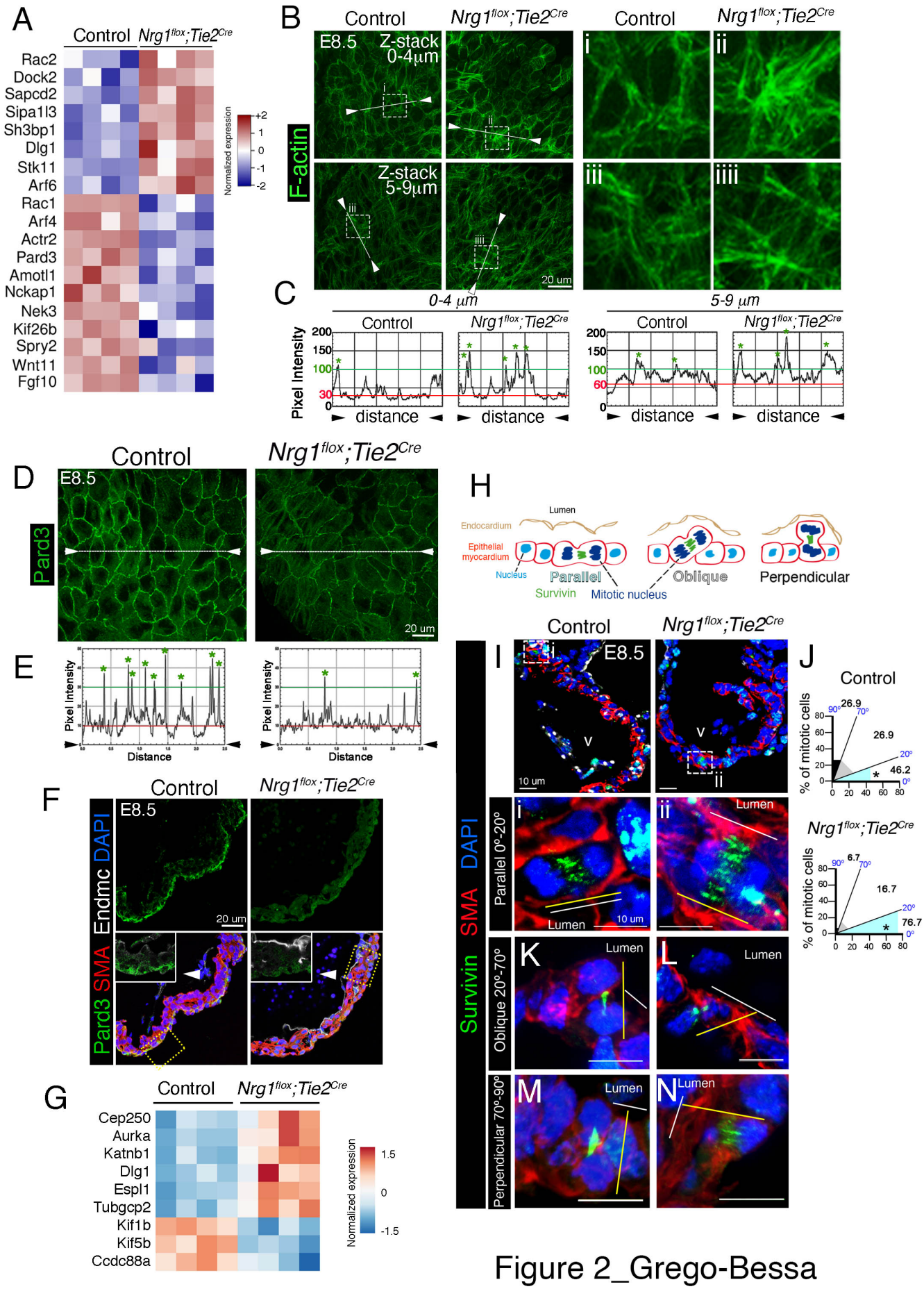

Figure 2_Grego-Bessa

747 **Figure 2. Nrg1 is required for polarity gene expression and cytoskeletal organization during**
748 **trabeculation. (A)** Enrichment analyses performed with Panther with the set of 1,219 differentially
749 expressed genes in a *Nrg1*^{flox}*;Tie2*^{Cre} vs control comparison, against the Biological Process GO term
750 database, identified "Establishment or maintenance of cell polarity" (GO:0007163) as enriched, with
751 *P* value=0.0064.. The heatmap represents relative expression values for differentially expressed genes
752 annotated with this GO term. **(B)** Whole mount phalloidin staining Z-stack projections of apical
753 regions (from 0 to 4 μm) and baso-lateral regions (5 to 9 μm) of outer compact myocardium in E8.5
754 control and *Nrg1*^{flox}*;Tie2*^{Cre} heart sections. **(C)** Quantification of pixel intensity along a 10-pixel-wide
755 trace (white lines in B). Red lines indicate that background intensities in control and *Nrg1*^{flox}*;Tie2*^{Cre}
756 heart sections are similar. Green asterisks indicate values above gray intensity=100 (green lines). **(D)**
757 Whole mount immunofluoresence of Pard3 in E8.5 control and *Nrg1*^{flox}*;Tie2*^{Cre} heart sections. **(E)**
758 Quantification of pixel intensity along a 10-pixel-wide trace (white lines between arrowheads). Red
759 lines indicate that background intensities in control and *Nrg1*^{flox}*;Tie2*^{Cre} heart sections are similar.
760 Green asterisks indicate values above gray intensity=30 (green lines). **(F)** Pard3 immunodetection in
761 transverse sections of E8.5 control and *Nrg1*^{flox}*;Tie2*^{Cre} embryos (green). Arrowheads to insets mark
762 the apical domain of the compact myocardium. SMA, smooth muscle actin; Endmc, endomucin
763 (white). DAPI counterstaining is shown in blue. **(G)** Heatmap of DEGs for components and regulators
764 of the mitotic spindle in E9.5 control vs. *Nrg1*^{flox}*;Tie2*^{Cre} heart expression profiles. The color code
765 represents normalized gene expression from -1.5 to +1.5. **(H)** Schematic of the analysis of mitotic-
766 spindle orientation relative to the cardiac lumen: parallel (0º – 20º), oblique (20º – 70º), or
767 perpendicular (70º – 90º). **(I)** Representative immunofluorescence images of mitotic cells stained
768 against Survivin (green) and SMA (red) in control and *Nrg1*^{flox}*;Tie2*^{Cre} heart sections at E8.5. DAPI
769 counterstaining is shown in blue. A general view of the E8.5 hearts is shown in the top panels. The
770 white lines below indicate the reference plane of the cardiac lumen. The yellow lines indicate the
771 orientation of the mitotic spindle. **(J)** Quantification of OCD in E8.5 control (N=3 embryos; n=26
772 mitotic figures) and *Nrg1*^{flox}*;Tie2*^{Cre} hearts (N=3 embryos; n=30 mitotic figures). *P* values were
773 obtained by Fisher's exact test. **P*-value < 0.05. Scale bars, 20 μm (B, D, F); 15 μm (D); 10 μm (I).

774

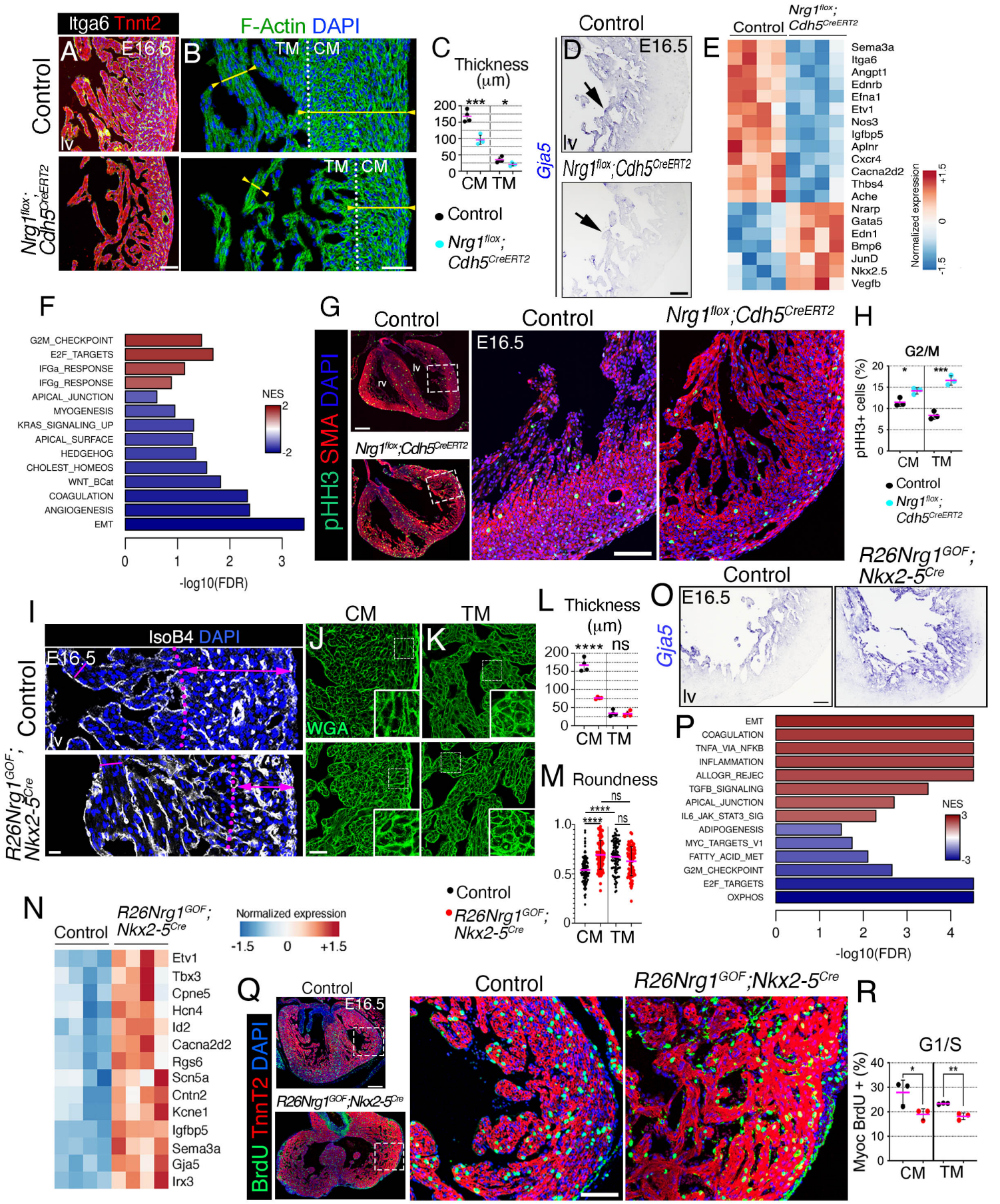

Figure 3_Grego-Bessa

775 **Figure 3. Nrg1 is required for trabecular growth, inner ventricular wall formation and its ectopic**
776 **expression blocks ventricular compaction. (A)** Immunofluorescence against integrin α6 (Itga6) and
777 Troponin T2 (Tnnt2) in control and *Nrg1*^{flox}*;Cdh5*^{CreERT2} heart transverse sections at E16.5. **(B)**
778 Phalloidin (F-Actin) staining in E16.5 control and *Nrg1*^{flox}*;Cdh5*^{CreERT2} heart sections. Dotted lines
779 mark the separation between compact and trabecular myocardium. CM, compact myocardium; TM,
780 trabecular myocardium. **(C)** Quantification of compact and trabecular myocardial thickness (n ≥3).
781 **(D)** ISH of *Gja5* in E16.5 control and *Nrg1*^{flox}*;Cdh5*^{CreERT2} embryos. Arrows mark trabecular
782 myocardium. lv, left ventricle. **(E)** Heatmap of representative DEGs in E15.5 control vs.
783 *Nrg1*^{flox}*;Cdh5*^{CreERT2} heart expression profiles. The color code represents normalized gene expression
784 from -1.5 to +1.5. **(F)** GSEA for E15.5 *Nrg1*^{flox}*;Cdh5*^{CreERT2} vs. Control, against Hallmark gene sets.
785 The bar plot represents enrichment data for 14 Hallmark gene sets at FDR qval < 0.25. Of these, 9 had
786 FDR qval < 0.05. Scale bar indicates normalized enrichment score (NES) from -2 to +2. Positive (red)
787 and negative (blue) scores, indicating enrichment or depletion, were found for 4 and 10 gene sets,
788 respectively. Relative expression values for the "leading edge" genes associated to gene sets EMT and
789 G2/M CHECKPOINT are presented as heatmaps in Figure S12. **(G)** left, phospho-histone 3 (pHH3)-
790 positive immunofluorescence on sections of E16.5 control and *Nrg1*^{flox}*;Cdh5*^{CreERT2} hearts (n=3 per
791 genotype); right, boxed regions magnified **(H)** Quantification of % pHH3-positive myocardial cells.
792 **(I)** DAPI staining in transverse sections of E16.5 control and *R26Nrg1*^{GOF}*;Nkx2-5*^{Cre} hearts. Double-
793 headed arrows in the high-magnification views indicate myocardium thickness. Dotted lines demark
794 the separation between CM and trabecular myocardium TM. **(J,K)** Wheat-germ-agglutinin (WGA)-
795 FITC staining on transverse sections of CM and TM in E16.5 control and *R26Nrg1*^{GOF}*;Nkx2-5*^{Cre}
796 hearts. **(L)** Quantification of CM and TM thickness in E16.5 control and *R26Nrg1*^{GOF}*;Nkx2-5*^{Cre} hearts
797 (n=3 per genotype). **(M)** Quantification of CM and TM cell roundness in E16.5 control and
798 *R26Nrg1*^{GOF}*;Nkx2-5*^{Cre} hearts sections (n=3 per genotype). **(N)** Heatmap of representative DEGs in
799 E15.5 *R26Nrg1*^{GOF}*;Nkx2-5*^{Cre} vs. control heart expression profiles. The color code represents
800 normalized gene expression from -1.5 to +1.5. **(O)** ISH for *Gja5* in E16.5 control and
801 *R26Nrg1*^{GOF}*;Nkx2-5*^{Cre} heart sections. **(P)** GSEA for E15.5 *R26Nrg1*^{GOF}*;Nkx2-5*^{Cre} vs. control, against
802 Hallmark gene sets. The bar plot represents enrichment data for a selection of 14 gene sets at FDR
803 qval < 0.05. Scale bar indicates normalized enrichment score (NES) from -3 to +3. Positive (red) and
804 negative (blue) scores, indicating enrichment or depletion, were found for 8 and 6 gene sets,
805 respectively. **(Q)** left, BrdU-positive immunofluorescence on sections of E16.5 control and
806 *R26Nrg1*^{GOF}*;Nkx2-5*^{Cre} hearts (n=3 per genotype); right, boxed regions magnified. **(R)** Quantification
807 of % BrdU incorporation in CM and TM in control and *R26Nrg1*^{GOF}*;Nkx2-5*^{Cre} hearts (n=3 per
808 genotype). **P*-value < 0.05, ** *P*< 0.01, *** *P* < 0.001, **** *P* < 0.0001, ns=non-significant by
809 Student t-test. Scale bars, 100 μm in A,D,O; 50 μm in B; 200 μm in G, 50 μm in G inset; 20 μm in I-
810 K; 200 μm in Q, 50 μm in inset.

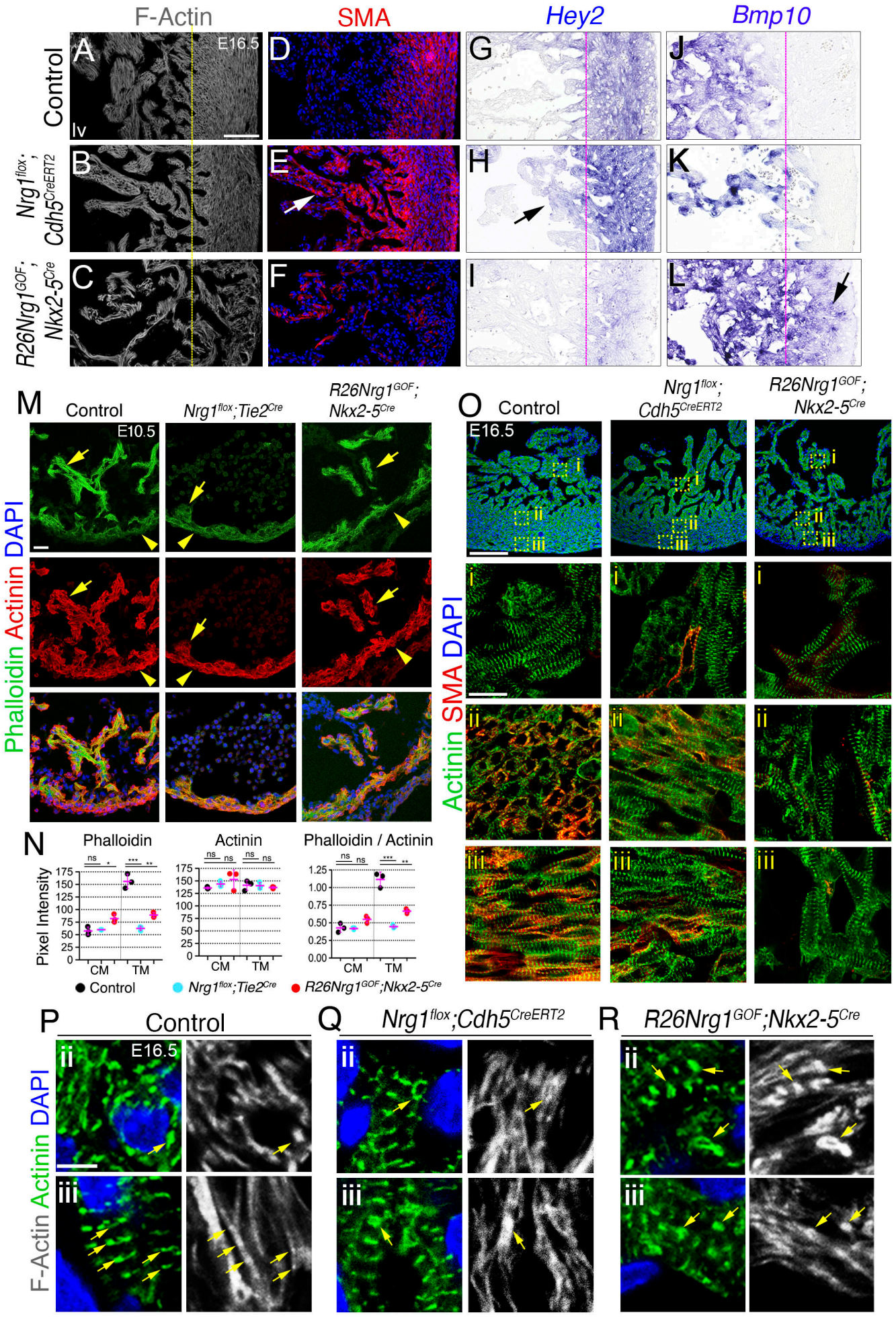

Figure 4_Grego-Bessa

811 **Figure 4. Ventricular patterning is mediated by cytoskeletal dynamics. (A-F)** Phalloidin (F-actin)
812 staining and immunodetection of smooth muscle actin (SMA) in E16.5 left ventricular sections from
813 control **(A, D)**, *Nrg1*^{flox}*;Cdh5*^{CreERT2} **(B, E)**, and *R26Nrg1*^{GOF}*;Nkx2-5*^{Cre} hearts **(C, F)**. Yellow lines
814 mark the position of the morphological border between trabecular myocardium (TM) and compact
815 myocardium (CM) in control heart sections, showing how this border shifts in *Nrg1*^{flox}*;Cdh5*^{CreERT2} and
816 *R26Nrg1*^{GOF}*;Nkx2-5*^{Cre} hearts. The arrow marks strong SMA immunostaining in TM relative to CM in
817 the *Nrg1*^{flox}*;Cdh5*^{Cre} heart. Note also the reduced SMA expression in CM of *R26Nrg1*^{GOF}*;Nkx2-5*^{Cre}
818 hearts **(F). (G-L)** ISH for *Hey2* and *BMP10* in E16.5 left ventricular sections from control **(G, J)**,
819 *Nrg1*^{flox}*;Cdh5*^{CreERT2} **(H, K)**, and *R26Nrg1*^{GOF}*;Nkx2-5-Cre* hearts **(I, L)**. Pink lines mark the position
820 of the morphological border between TM and CM in control heart sections, showing how this border
821 shifts in *Nrg1*^{flox}*;Cdh5*^{CreERT2} and *R26Nrg1*^{GOF}*;Nkx2-5*^{Cre} hearts. Arrows mark ectopic expression of
822 *Hey2* and *Bmp10* in *Nrg1*^{flox}*;Cdh5*^{CreERT2} and *R26Nrg1*^{GOF}*;Nkx2-5*^{Cre} hearts, respectively. Note also the
823 reduced *Hey2* expression in CM of *R26Nrg1*^{GOF}*;Nkx2-5*^{Cre} hearts. (**M**) F-actin (Phalloidin) and α-
824 actinin immunodetection in E10.5 control, *Nrg1*^{flox}*;Tie2*^{Cre} and *R26Nrg1*^{GOF}*;Nkx2-5*^{Cre} hearts. Yellow
825 arrows indicate TM and arrowheads CM. **(N)** Quantification of Phalloidin and α-actinin
826 immunofluorescence, and Phalloidin/α-actinin ratios in heart sections from E10.5 control,
827 *Nrg1*^{flox}*;Cdh5*^{CreERT2} and *R26Nrg1*^{GOF}*;Nkx2-5*^{Cre} embryos. **(O)** α-actinin and α-SMA immunodetection
828 in E16.5 control, *Nrg1*^{flox}*;Cdh5*^{CreERT2} and *R26Nrg1*^{GOF}*;Nkx2-5*^{Cre} hearts. Panels i, ii, and iii show high-
829 magnification views of TM, inner CM, and outer CM, respectively. **(P-R)** Detail of F-actin and α-
830 actinin double immunofluorescence at E16.5 in inner CM (ii) and outer CM (iii). Yellow arrows mark
831 Z-bands and highlight aberrant Z-band structures in *Nrg1*^{flox}*;Cdh5*^{CreERT2} and *R26Nrg1*^{GOF}*;Nkx2-5*^{Cre}
832 hearts. Scale bars, 100 μm in A-I,O; 20 μm in M; 10μm in O, i-iii; 5μm in P-R.

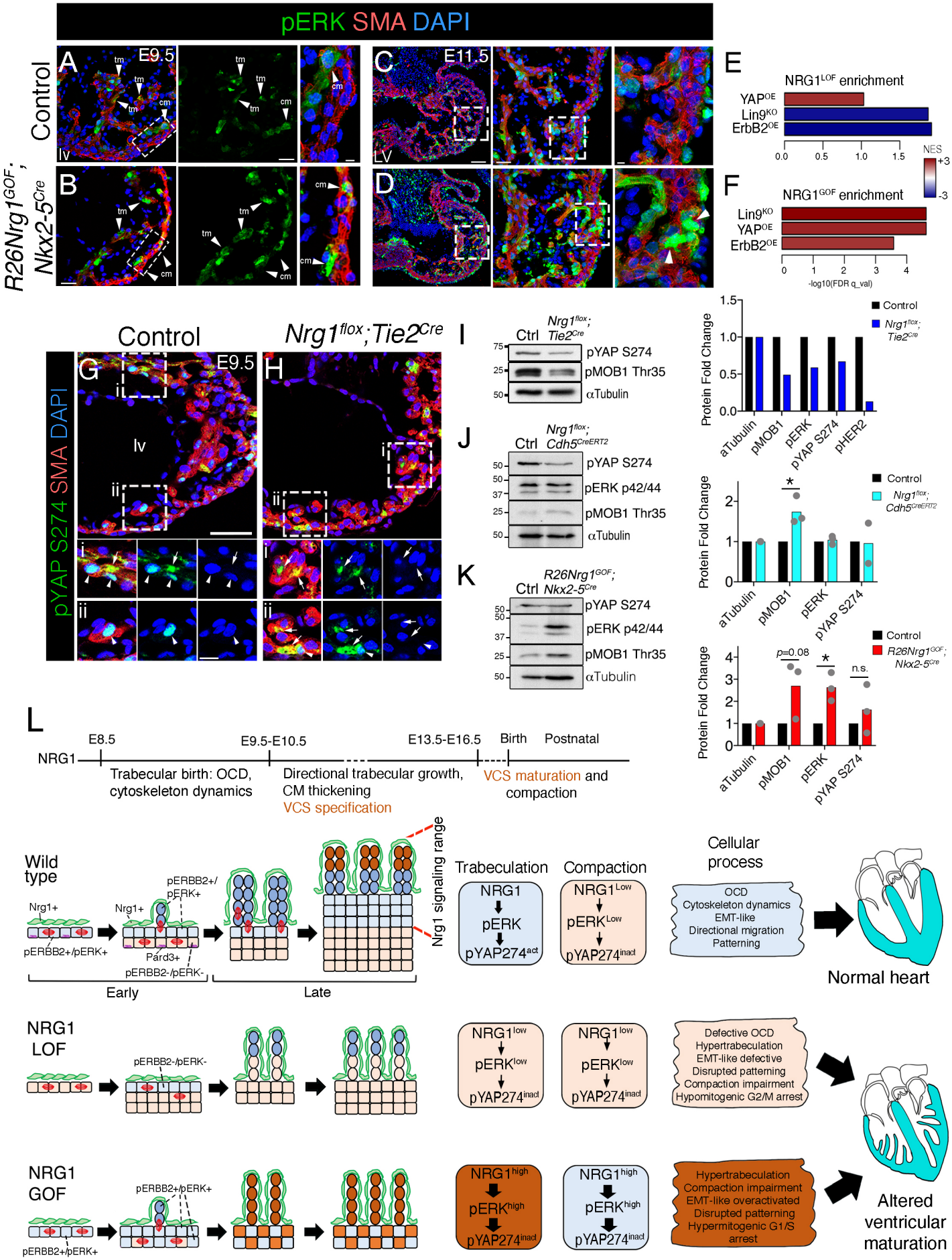

Figure 5_Grego-Bessa

833 **Figure 5. Ectopic pErk expression in *R26Nrg1^{GOF};Nkx2-5^{Cre}* compact myocardium and Nrg1-**
834 **dependent pYap1 S274 regulation during trabeculation. (A-C)** Immunofluorescence for pERK in
835 left ventricular sections from E9.5 **(A, B)** and E11.5 embryos **(C, D)**. Arrowheads mark labeled
836 cardiomyocytes in trabecular (tm) and compact (cm) myocardium. **(E)** GSEA for E15.5
837 *Nrg1^{flox};Cdh5^{CreERT2}* vs. Control and **(F)** E15.5 *R26Nrg1^{GOF};Nkx2-5^{Cre}* vs. Control, against gene sets
838 consisting of collections of differentially expressed genes derived from ERBB2^{OE} vs. Control [89] and
839 Lin9KO vs. Control[90], or direct YAP1-target genes[92]. The barplots represent enrichment data at FDR
840 qval < 0.25, and the color scale indicates normalized enrichment score (NES) from -3 to +3. **(G)**
841 Immunofluorescence detection of pYAP S274 in E9.5 control and **(H)** *Nrg1^{flox};Tie2^{Cre}* heart sections.
842 Arrows mark cytoplasmic signal, arrowheads nuclear signal. **(I)** Western blot analysis and
843 quantification of pYAP S274 and pMOB1 Thr35 in E9.5 control and *Nrg1^{flox};Tie2^{Cre}* ventricles (pool
844 of n=3 per genotype). **(J)** Western blot analysis of pYAP S274, pERK 42/44, and pMOB1 Thr35 in
845 E16.5 control and *Nrg1^{flox};Cdh5^{CreERT2}*, and **(K)** control and *R26Nrg1^{GOF};Nkx2-5^{Cre}* ventricles (n=1 per
846 genotype), and quantifications (n=2-3). **P*-value < 0.05, ns=non-significant by Student t-
847 testα–Tubulin was used as a gel-loading control and for normalization in quantifications. Scale bars,
848 100 μm, 20 μm, and 10 μm from low to high magnification view in A, B; 100 μm, 30 μm, and 10 μm
849 in C, D; 50 μm in G,H; i,ii, 10 μm**.** **(L)** Nrg1 regulates cardiomyocyte dynamics, cell cycle
850 progression, and maturation during ventricular chamber morphogenesis. Wild type (E8.5-E10.5), the
851 early myocardium is characterized by parallel divisions in the outer myocardial layer and
852 perpendicular cell divisions in the inner myocardial layer. Nrg1 released from the endocardium (cells
853 in green) activates pErbB2 and pErk in the trabecular layer (cells in blue), promoting pYap S274
854 nuclear localization (pYap S274^{act}). This signaling is associated with the activation of actin
855 cytoskeleton, EMT-like dynamics, directional migration, and chamber patterning (compact vs.
856 trabecular). Nrg1 LOF (E8.5-E10.5), deficient Nrg1 signaling leads to reduced perpendicular divisions
857 in favor of parallel ones (defective OCD), causing compact myocardium thickening and trabeculae
858 underdevelopment. These changes are associated with the depletion of apico-basal polarity markers,
859 disorganized actin cytoskeleton, low pErk and pYap S274 inactivation (pYap S274^{inact}). Wild-type
860 (E10.5-E16.5), trabeculae elongate by directional migration from the proliferative outer compact
861 myocardium (cells in beige) towards the inner compact myocardium (cells in blue). Nrg1 is required
862 for specification of the ventricular conduction system (VCS) in trabeculae (brown cells) but not for
863 compaction in late gestation or postnatally. LOF (E10.5-E16.5), Nrg1 depletion and low pErk,
864 trabecular myocardium expresses compact myocardium genes, leading to rudimentary and mis-
865 patterned trabeculae, blunted inner myocardial wall growth, and hypomitogenic cell cycle arrest. GOF
866 (E10.5-E16.5), cardiac Nrg1 overexpression and high pErk, disrupts patterning by trabeculating the
867 compact myocardium and impairing compaction. Hypermitogenic signaling causes cell cycle arrest in

868 cardiomyocytes and onset of senescence. Both Nrg1 LOF and GOF lead to altered ventricular chamber
869 maturation and cardiac developmental arrest.
870
871 **References**
872

873 **1.** Jimenez-Amilburu V, Rasouli SJ, Staudt DW, Nakajima H, Chiba A, Mochizuki N,
874 Stainier DY. In Vivo Visualization of Cardiomyocyte Apicobasal Polarity Reveals
875 Epithelial to Mesenchymal-like Transition during Cardiac Trabeculation. *Cell Rep.*
876 2016;17:2687-2699.

877 **2.** Lee J, Vedula V, Baek KI, Chen J, Hsu JJ, Ding Y, Chang CC, Kang H, Small A, Fei P,
878 Chuong CM, Li R, Demer L, Packard RRS, Marsden AL, Hsiai TK. Spatial and temporal
879 variations in hemodynamic forces initiate cardiac trabeculation. *JCI Insight.* 2018;3.

880 **3.** Liu J, Bressan M, Hassel D, Huisken J, Staudt D, Kikuchi K, Poss KD, Mikawa T,
881 Stainier DY. A dual role for ErbB2 signaling in cardiac trabeculation. *Development.*
882 2010;137:3867-3875.

883 **4.** Peshkovsky C, Totong R, Yelon D. Dependence of cardiac trabeculation on neuregulin
884 signaling and blood flow in zebrafish. *Dev Dyn.* 2011;240:446-456.

885 **5.** Priya R, Allanki S, Gentile A, Mansingh S, Uribe V, Maischein HM, Stainier DYR.
886 Tension heterogeneity directs form and fate to pattern the myocardial wall. *Nature.*
887 2020;588:130-134.

888 **6.** Li J, Miao L, Shieh D, Spiotto E, Li J, Zhou B, Paul A, Schwartz RJ, Firulli AB, Singer
889 HA, Huang G, Wu M. Single-Cell Lineage Tracing Reveals that Oriented Cell Division
890 Contributes to Trabecular Morphogenesis and Regional Specification. *Cell Rep.*
891 2016;15:158-170.

892 **7.** Miao L, Li J, Li J, Lu Y, Shieh D, Mazurkiewicz JE, Barroso M, Schwarz JJ, Xin HB,
893 Singer HA, Vincent PA, Zhong W, Radice GL, Wan LQ, Fan ZC, Huang G, Wu M.
894 Cardiomyocyte orientation modulated by the Numb family proteins-N-cadherin axis is
895 essential for ventricular wall morphogenesis. *Proc Natl Acad Sci U S A.* 2019;116:15560-
896 15569.

897 **8.** Yue Y, Zong W, Li X, Li J, Zhang Y, Wu R, Liu Y, Cui J, Wang Q, Bian Y, Yu X, Liu
898 Y, Tan G, Zhang Y, Zhao G, Zhou B, Chen L, Xiao W, Cheng H, He A. Long-term, in
899 toto live imaging of cardiomyocyte behaviour during mouse ventricle chamber formation
900 at single-cell resolution. *Nat Cell Biol.* 2020;22:332-340.

901 **9.** Sedmera D, Pexieder T, Vuillemin M, Thompson RP, Anderson RH. Developmental
902 patterning of the myocardium. *Anat Rec.* 2000;258:319-337.

903 **10.** Gourdie RG, Mima T, Thompson RP, Mikawa T. Terminal diversification of the myocyte
904 lineage generates Purkinje fibers of the cardiac conduction system. *Development.*
905 1995;121:1423-1431.

906 **11.** Moorman AF, Christoffels VM. Cardiac chamber formation: development, genes, and
907 evolution. *Physiol Rev.* 2003;83:1223-1267.

908 **12.** Tian X, Hu T, Zhang H, He L, Huang X, Liu Q, Yu W, He L, Yang Z, Yan Y, Yang X,
909 Zhong TP, Pu WT, Zhou B. Vessel formation. De novo formation of a distinct coronary
910 vascular population in neonatal heart. *Science.* 2014;345:90-94.

911 **13.** Tian X, Li Y, He L, Zhang H, Huang X, Liu Q, Pu W, Zhang L, Li Y, Zhao H, Wang Z,
912 Zhu J, Nie Y, Hu S, Sedmera D, Zhong TP, Yu Y, Zhang L, Yan Y, Qiao Z, Wang QD,
913 Wu SM, Pu WT, Anderson RH, Zhou B. Identification of a hybrid myocardial zone in
914 the mammalian heart after birth. *Nat Commun.* 2017;8:87.

915 **14.** Wu B, Zhang Z, Lui W, Chen X, Wang Y, Chamberlain AA, Moreno-Rodriguez RA,
916 Markwald RR, O'Rourke BP, Sharp DJ, Zheng D, Lenz J, Baldwin HS, Chang CP, Zhou
917 B. Endocardial cells form the coronary arteries by angiogenesis through myocardial-
918 endocardial VEGF signaling. *Cell.* 2012;151:1083-1096.

919 **15.** Choquet C, Kelly RG, Miquerol L. Defects in Trabecular Development Contribute to Left
920 Ventricular Noncompaction. *Pediatr Cardiol.* 2019;40:1331-1338.

921 **16.** Finsterer J, Stollberger C, Towbin JA. Left ventricular noncompaction cardiomyopathy:
922 cardiac, neuromuscular, and genetic factors. *Nat Rev Cardiol.* 2017;14:224-237.

923 **17.** Arbustini E, Weidemann F, Hall JL. Left ventricular noncompaction: a distinct
924 cardiomyopathy or a trait shared by different cardiac diseases? *J Am Coll Cardiol.*
925 2014;64:1840-1850.

926 **18.** Abela M, D'Silva A. Left Ventricular Trabeculations in Athletes: Epiphenomenon or
927 Phenotype of Disease? *Curr Treat Options Cardiovasc Med.* 2018;20:100.

928 **19.** Meyer HV, Dawes TJW, Serrani M, Bai W, Tokarczuk P, Cai J, de Marvao A, Henry A,
929 Lumbers RT, Gierten J, Thumberger T, Wittbrodt J, Ware JS, Rueckert D, Matthews PM,
930 Prasad SK, Costantino ML, Cook SA, Birney E, O'Regan DP. Genetic and functional
931 insights into the fractal structure of the heart. *Nature.* 2020;584:589-594.

932 **20.** Anderson RH, Jensen B, Mohun TJ, Petersen SE, Aung N, Zemrak F, Planken RN,
933 MacIver DH. Key Questions Relating to Left Ventricular Noncompaction
934 Cardiomyopathy: Is the Emperor Still Wearing Any Clothes? *Can J Cardiol.*
935 2017;33:747-757.

936 **21.** Oechslin E, Jenni R, Klaassen S. Left Ventricular Noncompaction Is a Myocardial
937 Phenotype: Cardiomyopathy-Yes or No? *Can J Cardiol.* 2021;37:366-369.

938 **22.** Weir-McCall JR, Yeap PM, Papagiorcopulo C, Fitzgerald K, Gandy SJ, Lambert M,
939 Belch JJ, Cavin I, Littleford R, Macfarlane JA, Matthew SZ, Nicholas RS, Struthers AD,
940 Sullivan F, Waugh SA, White RD, Houston JG. Left Ventricular Noncompaction:
941 Anatomical Phenotype or Distinct Cardiomyopathy? *J Am Coll Cardiol.* 2016;68:2157-
942 2165.

943 **23.** Lai D, Liu X, Forrai A, Wolstein O, Michalicek J, Ahmed I, Garratt AN, Birchmeier C,
944 Zhou M, Hartley L, Robb L, Feneley MP, Fatkin D, Harvey RP. Neuregulin 1 sustains
945 the gene regulatory network in both trabecular and nontrabecular myocardium. *Circ Res.*
946 2010;107:715-727.

947 **24.** Meyer D, Birchmeier C. Multiple essential functions of neuregulin in development.
948 *Nature.* 1995;378:386-390.

949 **25.** Rasouli SJ, Stainier DYR. Regulation of cardiomyocyte behavior in zebrafish
950 trabeculation by Neuregulin 2a signaling. *Nat Commun.* 2017;8:15281.

951 **26.** Sanchez-Soria P, Camenisch TD. ErbB signaling in cardiac development and disease.
952 *Semin Cell Dev Biol.* 2010;21:929-935.

953 **27.** Baliga RR, Pimental DR, Zhao YY, Simmons WW, Marchionni MA, Sawyer DB, Kelly
954 RA. NRG-1-induced cardiomyocyte hypertrophy. Role of PI-3-kinase, p70(S6K), and
955 MEK-MAPK-RSK. *Am J Physiol.* 1999;277:H2026-2037.

956 **28.** Del Monte-Nieto G, Ramialison M, Adam AAS, Wu B, Aharonov A, D'Uva G, Bourke
957 LM, Pitulescu ME, Chen H, de la Pompa JL, Shou W, Adams RH, Harten SK, Tzahor E,
958 Zhou B, Harvey RP. Control of cardiac jelly dynamics by NOTCH1 and NRG1 defines
959 the building plan for trabeculation. *Nature.* 2018;557:439-445.

960 **29.** Gassmann M, Casagranda F, Orioli D, Simon H, Lai C, Klein R, Lemke G. Aberrant
961 neural and cardiac development in mice lacking the ErbB4 neuregulin receptor. *Nature.*
962 1995;378:390-394.

963 **30.** Kramer R, Bucay N, Kane DJ, Martin LE, Tarpley JE, Theill LE. Neuregulins with an
964 Ig-like domain are essential for mouse myocardial and neuronal development. *Proc Natl*
965 *Acad Sci U S A.* 1996;93:4833-4838.

966 **31.** Lai JKH, Collins MM, Uribe V, Jimenez-Amilburu V, Gunther S, Maischein HM,
967 Stainier DYR. The Hippo pathway effector Wwtr1 regulates cardiac wall maturation in
968 zebrafish. *Development.* 2018;145.

969 **32.** Lee KF, Simon H, Chen H, Bates B, Hung MC, Hauser C. Requirement for neuregulin
970 receptor erbB2 in neural and cardiac development. *Nature.* 1995;378:394-398.

971 **33.** Bersell K, Arab S, Haring B, Kuhn B. Neuregulin1/ErbB4 signaling induces
972 cardiomyocyte proliferation and repair of heart injury. *Cell.* 2009;138:257-270.

973 **34.** D'Uva G, Aharonov A, Lauriola M, Kain D, Yahalom-Ronen Y, Carvalho S, Weisinger
974 K, Bassat E, Rajchman D, Yifa O, Lysenko M, Konfino T, Hegesh J, Brenner O, Neeman
975 M, Yarden Y, Leor J, Sarig R, Harvey RP, Tzahor E. ERBB2 triggers mammalian heart
976 regeneration by promoting cardiomyocyte dedifferentiation and proliferation. *Nat Cell*
977 *Biol.* 2015;17:627-638.

978 **35.** Polizzotti BD, Ganapathy B, Walsh S, Choudhury S, Ammanamanchi N, Bennett DG,
979 dos Remedios CG, Haubner BJ, Penninger JM, Kuhn B. Neuregulin stimulation of
980 cardiomyocyte regeneration in mice and human myocardium reveals a therapeutic
981 window. *Sci Transl Med.* 2015;7:281ra245.

982 **36.** Liu X, Gu X, Li Z, Li X, Li H, Chang J, Chen P, Jin J, Xi B, Chen D, Lai D, Graham
983 RM, Zhou M. Neuregulin-1/erbB-activation improves cardiac function and survival in
984 models of ischemic, dilated, and viral cardiomyopathy. *J Am Coll Cardiol.* 2006;48:1438-
985 1447.

986 **37.** Gao R, Zhang J, Cheng L, Wu X, Dong W, Yang X, Li T, Liu X, Xu Y, Li X, Zhou M.
987 A Phase II, randomized, double-blind, multicenter, based on standard therapy, placebo-
988 controlled study of the efficacy and safety of recombinant human neuregulin-1 in patients
989 with chronic heart failure. *J Am Coll Cardiol.* 2010;55:1907-1914.

990 **38.** Jabbour A, Hayward CS, Keogh AM, Kotlyar E, McCrohon JA, England JF, Amor R,
991 Liu X, Li XY, Zhou MD, Graham RM, Macdonald PS. Parenteral administration of
992 recombinant human neuregulin-1 to patients with stable chronic heart failure produces

993 favourable acute and chronic haemodynamic responses. *Eur J Heart Fail.* 2011;13:83-
994 92.

995 **39.** Sawyer DB, Caggiano A. Neuregulin-1beta for the treatment of systolic heart failure. *J*
996 *Mol Cell Cardiol.* 2011;51:501-505.

997 **40.** Geissler A, Ryzhov S, Sawyer DB. Neuregulins: protective and reparative growth factors
998 in multiple forms of cardiovascular disease. *Clin Sci (Lond).* 2020;134:2623-2643.

999 **41.** Zhang W, Chen H, Qu X, Chang CP, Shou W. Molecular mechanism of ventricular
1000 trabeculation/compaction and the pathogenesis of the left ventricular noncompaction
1001 cardiomyopathy (LVNC). *Am J Med Genet C Semin Med Genet.* 2013;163C:144-156.

1002 **42.** Yang X, Arber S, William C, Li L, Tanabe Y, Jessell TM, Birchmeier C, Burden SJ.
1003 Patterning of muscle acetylcholine receptor gene expression in the absence of motor
1004 innervation. *Neuron.* 2001;30:399-410.

1005 **43.** Kisanuki YY, Hammer RE, Miyazaki J, Williams SC, Richardson JA, Yanagisawa M.
1006 Tie2-Cre transgenic mice: a new model for endothelial cell-lineage analysis in vivo. *Dev*
1007 *Biol.* 2001;230:230-242.

1008 **44.** Saga Y, Miyagawa-Tomita S, Takagi A, Kitajima S, Miyazaki J, Inoue T. MesP1 is
1009 expressed in the heart precursor cells and required for the formation of a single heart tube.
1010 *Development.* 1999;126:3437-3447.

1011 **45.** Liu FF, Stone JR, Schuldt AJ, Okoshi K, Okoshi MP, Nakayama M, Ho KK, Manning
1012 WJ, Marchionni MA, Lorell BH, Morgan JP, Yan X. Heterozygous knockout of
1013 neuregulin-1 gene in mice exacerbates doxorubicin-induced heart failure. *Am J Physiol*
1014 *Heart Circ Physiol.* 2005;289:H660-666.

1015 **46.** Camenisch TD, Schroeder JA, Bradley J, Klewer SE, McDonald JA. Heart-valve
1016 mesenchyme formation is dependent on hyaluronan-augmented activation of ErbB2-
1017 ErbB3 receptors. *Nat Med.* 2002;8:850-855.

1018 **47.** Li G, Tian L, Goodyer W, Kort EJ, Buikema JW, Xu A, Wu JC, Jovinge S, Wu SM.
1019 Single cell expression analysis reveals anatomical and cell cycle-dependent
1020 transcriptional shifts during heart development. *Development.* 2019;146.

1021 **48.** Liberzon A, Birger C, Thorvaldsdottir H, Ghandi M, Mesirov JP, Tamayo P. The
1022 Molecular Signatures Database (MSigDB) hallmark gene set collection. *Cell Syst.*
1023 2015;1:417-425.

1024 **49.** Harris SL, Levine AJ. The p53 pathway: positive and negative feedback loops. *Oncogene.*
1025 2005;24:2899-2908.

1026 **50.** Toyoshima H, Hunter T. p27, a novel inhibitor of G1 cyclin-Cdk protein kinase activity,
1027 is related to p21. *Cell.* 1994;78:67-74.

1028 **51.** Kiyokawa H, Kineman RD, Manova-Todorova KO, Soares VC, Hoffman ES, Ono M,
1029 Khanam D, Hayday AC, Frohman LA, Koff A. Enhanced growth of mice lacking the
1030 cyclin-dependent kinase inhibitor function of p27(Kip1). *Cell.* 1996;85:721-732.

1031 **52.** Nakayama K, Ishida N, Shirane M, Inomata A, Inoue T, Shishido N, Horii I, Loh DY,
1032 Nakayama K. Mice lacking p27(Kip1) display increased body size, multiple organ
1033 hyperplasia, retinal dysplasia, and pituitary tumors. *Cell.* 1996;85:707-720.

1034 **53.** Staudt DW, Liu J, Thorn KS, Stuurman N, Liebling M, Stainier DY. High-resolution
1035 imaging of cardiomyocyte behavior reveals two distinct steps in ventricular trabeculation.
1036 *Development.* 2014;141:585-593.

1037 **54.** Li R, Gundersen GG. Beyond polymer polarity: how the cytoskeleton builds a polarized
1038 cell. *Nat Rev Mol Cell Biol.* 2008;9:860-873.

1039 **55.** Cherian AV, Fukuda R, Augustine SM, Maischein HM, Stainier DY. N-cadherin
1040 relocalization during cardiac trabeculation. *Proc Natl Acad Sci U S A.* 2016;113:7569-
1041 7574.

1042 **56.** Passer D, van de Vrugt A, Atmanli A, Domian IJ. Atypical Protein Kinase C-Dependent
1043 Polarized Cell Division Is Required for Myocardial Trabeculation. *Cell Rep.*
1044 2016;14:1662-1672.

1045 **57.** McCaffrey LM, Macara IG. Signaling pathways in cell polarity. *Cold Spring Harb*
1046 *Perspect Biol.* 2012;4.

1047 **58.** Hikita T, Mirzapourshafiyi F, Barbacena P, Riddell M, Pasha A, Li M, Kawamura T,
1048 Brandes RP, Hirose T, Ohno S, Gerhardt H, Matsuda M, Franco CA, Nakayama M. PAR-
1049 3 controls endothelial planar polarity and vascular inflammation under laminar flow.
1050 *EMBO Rep.* 2018;19.

1051 **59.** Jimenez-Amilburu V, Stainier DYR. The transmembrane protein Crb2a regulates
1052 cardiomyocyte apicobasal polarity and adhesion in zebrafish. *Development.* 2019;146.

1053 **60.** di Pietro F, Echard A, Morin X. Regulation of mitotic spindle orientation: an integrated
1054 view. *EMBO Rep.* 2016;17:1106-1130.

1055 **61.** Wang Y, Nakayama M, Pitulescu ME, Schmidt TS, Bochenek ML, Sakakibara A, Adams
1056 S, Davy A, Deutsch U, Luthi U, Barberis A, Benjamin LE, Makinen T, Nobes CD, Adams
1057 RH. Ephrin-B2 controls VEGF-induced angiogenesis and lymphangiogenesis. *Nature.*
1058 2010;465:483-486.

1059 **62.** Ivins S, Chappell J, Vernay B, Suntharalingham J, Martineau A, Mohun TJ, Scambler PJ.
1060 The CXCL12/CXCR4 Axis Plays a Critical Role in Coronary Artery Development. *Dev*
1061 *Cell.* 2015;33:455-468.

1062 **63.** Kwon HB, Wang S, Helker CS, Rasouli SJ, Maischein HM, Offermanns S, Herzog W,
1063 Stainier DY. In vivo modulation of endothelial polarization by Apelin receptor signalling.
1064 *Nat Commun.* 2016;7:11805.

1065 **64.** Rasanen M, Sultan I, Paech J, Hemanthakumar KA, Yu W, He L, Tang J, Sun Y,
1066 Hlushchuk R, Huan X, Armstrong E, Khoma OZ, Mervaala E, Djonov V, Betsholtz C,
1067 Zhou B, Kivela R, Alitalo K. VEGF-B Promotes Endocardium-Derived Coronary Vessel
1068 Development and Cardiac Regeneration. *Circulation.* 2021;143:65-77.

1069 **65.** Suri C, Jones PF, Patan S, Bartunkova S, Maisonpierre PC, Davis S, Sato TN,
1070 Yancopoulos GD. Requisite role of angiopoietin-1, a ligand for the TIE2 receptor, during
1071 embryonic angiogenesis. *Cell.* 1996;87:1171-1180.

1072 **66.** Li Y, Tian X, Zhao H, He L, Zhang S, Huang X, Zhang H, Miquerol L, Zhou B. Genetic
1073 targeting of Purkinje fibres by Sema3a-CreERT2. *Sci Rep.* 2018;8:2382.

1074 **67.** Klein R. Eph/ephrin signalling during development. *Development.* 2012;139:4105-4109.

1075 **68.** Munshi NV. Gene regulatory networks in cardiac conduction system development. *Circ*
1076 *Res.* 2012;110:1525-1537.

1077 **69.** Shekhar A, Lin X, Liu FY, Zhang J, Mo H, Bastarache L, Denny JC, Cox NJ, Delmar M,
1078 Roden DM, Fishman GI, Park DS. Transcription factor ETV1 is essential for rapid
1079 conduction in the heart. *J Clin Invest.* 2016;126:4444-4459.

1080 **70.** Sun Q, Liu S, Liu K, Jiao K. Role of Semaphorin Signaling During Cardiovascular
1081 Development. *J Am Heart Assoc.* 2018;7.

1082 **71.** Lu P, Wu B, Wang Y, Russell M, Liu Y, Bernard DJ, Zheng D, Zhou B. Prerequisite
1083 endocardial-mesenchymal transition for murine cardiac trabecular angiogenesis. *Dev*
1084 *Cell.* 2023;58:791-805 e794.

1085 **72.** Travisano SI, Oliveira VL, Prados B, Grego-Bessa J, Pineiro-Sabaris R, Bou V, Gomez
1086 MJ, Sanchez-Cabo F, MacGrogan D, de la Pompa JL. Coronary arterial development is
1087 regulated by a Dll4-Jag1-EphrinB2 signaling cascade. *Elife.* 2019;8:1-30.

1088 **73.** Claxton S, Kostourou V, Jadeja S, Chambon P, Hodivala-Dilke K, Fruttiger M. Efficient,
1089 inducible Cre-recombinase activation in vascular endothelium. *Genesis.* 2008;46:74-80.

1090 **74.** Sharma B, Ho L, Ford GH, Chen HI, Goldstone AB, Woo YJ, Quertermous T, Reversade
1091 B, Red-Horse K. Alternative Progenitor Cells Compensate to Rebuild the Coronary
1092 Vasculature in Elabela- and Apj-Deficient Hearts. *Dev Cell.* 2017;42:655-666 e653.

1093 **75.** Haskins JW, Nguyen DX, Stern DF. Neuregulin 1-activated ERBB4 interacts with YAP
1094 to induce Hippo pathway target genes and promote cell migration. *Sci Signal.*
1095 2014;7:ra116.

1096 **76.** Lavoie H, Gagnon J, Therrien M. ERK signalling: a master regulator of cell behaviour,
1097 life and fate. *Nat Rev Mol Cell Biol.* 2020;21:607-632.

1098 **77.** Wang Z. Regulation of Cell Cycle Progression by Growth Factor-Induced Cell Signaling.
1099 *Cells.* 2021;10.

1100 **78.** Payne SR, Zhang S, Tsuchiya K, Moser R, Gurley KE, Longton G, deBoer J, Kemp CJ.
1101 p27kip1 deficiency impairs G2/M arrest in response to DNA damage, leading to an
1102 increase in genetic instability. *Mol Cell Biol.* 2008;28:258-268.

1103 **79.** Goodyer WR, Beyersdorf BM, Paik DT, Tian L, Li G, Buikema JW, Chirikian O, Choi
1104 S, Venkatraman S, Adams EL, Tessier-Lavigne M, Wu JC, Wu SM. Transcriptomic
1105 Profiling of the Developing Cardiac Conduction System at Single-Cell Resolution. *Circ*
1106 *Res.* 2019;125:379-397.

1107 **80.** Rentschler S, Zander J, Meyers K, France D, Levine R, Porter G, Rivkees SA, Morley
1108 GE, Fishman GI. Neuregulin-1 promotes formation of the murine cardiac conduction
1109 system. *Proc Natl Acad Sci U S A.* 2002;99:10464-10469.

1110 **81.** Redmond CJ, Coulombe PA. Intermediate filaments as effectors of differentiation. *Curr*
1111 *Opin Cell Biol.* 2021;68:155-162.

1112 **82.** Hertig V, Matos-Nieves A, Garg V, Villeneuve L, Mamarbachi M, Caland L, Calderone
1113 A. Nestin expression is dynamically regulated in cardiomyocytes during embryogenesis.
1114 *J Cell Physiol.* 2018;233:3218-3229.

1115 **83.** Calcinotto A, Kohli J, Zagato E, Pellegrini L, Demaria M, Alimonti A. Cellular
1116 Senescence: Aging, Cancer, and Injury. *Physiol Rev.* 2019;99:1047-1078.

1117 **84.** Blagosklonny MV. Cell senescence and hypermitogenic arrest. *EMBO Rep.* 2003;4:358-
1118 362.

1119 **85.** Nakayama K, Nagahama H, Minamishima YA, Miyake S, Ishida N, Hatakeyama S,
1120 Kitagawa M, Iemura S, Natsume T, Nakayama KI. Skp2-mediated degradation of p27
1121 regulates progression into mitosis. *Dev Cell.* 2004;6:661-672.

1122 **86.** Hnit SS, Xie C, Yao M, Holst J, Bensoussan A, De Souza P, Li Z, Dong Q. p27(Kip1)
1123 signaling: Transcriptional and post-translational regulation. *Int J Biochem Cell Biol.*
1124 2015;68:9-14.

1125 **87.** Ya J, Markman MW, Wagenaar GT, Blommaart PJ, Moorman AF, Lamers WH.
1126 Expression of the smooth-muscle proteins alpha-smooth-muscle actin and calponin, and
1127 of the intermediate filament protein desmin are parameters of cardiomyocyte maturation
1128 in the prenatal rat heart. *Anat Rec.* 1997;249:495-505.

1129 **88.** Clarke DN, Martin AC. Actin-based force generation and cell adhesion in tissue
1130 morphogenesis. *Curr Biol.* 2021;31:R667-R680.

1131 **89.** Aharonov A, Shakked A, Umansky KB, Savidor A, Genzelinakh A, Kain D, Lendengolts
1132 D, Revach OY, Morikawa Y, Dong J, Levin Y, Geiger B, Martin JF, Tzahor E. ERBB2
1133 drives YAP activation and EMT-like processes during cardiac regeneration. *Nat Cell*
1134 *Biol.* 2020;22:1346-1356.

1135 **90.** Grundl M, Walz S, Hauf L, Schwab M, Werner KM, Spahr S, Schulte C, Maric HM, Ade
1136 CP, Gaubatz S. Interaction of YAP with the Myb-MuvB (MMB) complex defines a
1137 transcriptional program to promote the proliferation of cardiomyocytes. *PLoS Genet.*
1138 2020;16:e1008818.

1139 **91.** Pattschull G, Walz S, Grundl M, Schwab M, Ruhl E, Baluapuri A, Cindric-Vranesic A,
1140 Kneitz S, Wolf E, Ade CP, Rosenwald A, von Eyss B, Gaubatz S. The Myb-MuvB
1141 Complex Is Required for YAP-Dependent Transcription of Mitotic Genes. *Cell Rep.*
1142 2019;27:3533-3546 e3537.

1143 **92.** Monroe TO, Hill MC, Morikawa Y, Leach JP, Heallen T, Cao S, Krijger PHL, de Laat
1144 W, Wehrens XHT, Rodney GG, Martin JF. YAP Partially Reprograms Chromatin
1145 Accessibility to Directly Induce Adult Cardiogenesis In Vivo. *Dev Cell.* 2019;48:765-
1146 779 e767.

1147 **93.** Yang S, Zhang L, Liu M, Chong R, Ding SJ, Chen Y, Dong J. CDK1 phosphorylation of
1148 YAP promotes mitotic defects and cell motility and is essential for neoplastic
1149 transformation. *Cancer Res.* 2013;73:6722-6733.

1150 **94.** Vlahov N, Scrace S, Soto MS, Grawenda AM, Bradley L, Pankova D, Papaspyropoulos
1151 A, Yee KS, Buffa F, Goding CR, Timpson P, Sibson N, O'Neill E. Alternate RASSF1
1152 Transcripts Control SRC Activity, E-Cadherin Contacts, and YAP-Mediated Invasion.
1153 *Curr Biol.* 2015;25:3019-3034.

1154 **95.** Gupta V, Poss KD. Clonally dominant cardiomyocytes direct heart morphogenesis.
1155 *Nature.* 2012;484:479-484.

1156 **96.** Barak Y, Hemberger M, Sucov HM. Phases and Mechanisms of Embryonic
1157 Cardiomyocyte Proliferation and Ventricular Wall Morphogenesis. *Pediatr Cardiol.*
1158 2019;40:1359-1366.

1159 **97.** Meilhac SM, Kelly RG, Rocancourt D, Eloy-Trinquet S, Nicolas JF, Buckingham ME.
1160 A retrospective clonal analysis of the myocardium reveals two phases of clonal growth
1161 in the developing mouse heart. *Development.* 2003;130:3877-3889.

1162 **98.** Ong LL, Kim N, Mima T, Cohen-Gould L, Mikawa T. Trabecular myocytes of the
1163 embryonic heart require N-cadherin for migratory unit identity. *Dev Biol.* 1998;193:1-9.

1164 **99.** Yang J, Antin P, Berx G, Blanpain C, Brabletz T, Bronner M, Campbell K, Cano A,
1165 Casanova J, Christofori G, Dedhar S, Derynck R, Ford HL, Fuxe J, Garcia de Herreros
1166 A, Goodall GJ, Hadjantonakis AK, Huang RYJ, Kalcheim C, Kalluri R, Kang Y, Khew-
1167 Goodall Y, Levine H, Liu J, Longmore GD, Mani SA, Massague J, Mayor R, McClay D,
1168 Mostov KE, Newgreen DF, Nieto MA, Puisieux A, Runyan R, Savagner P, Stanger B,
1169 Stemmler MP, Takahashi Y, Takeichi M, Theveneau E, Thiery JP, Thompson EW,
1170 Weinberg RA, Williams ED, Xing J, Zhou BP, Sheng G, Association EMTI. Guidelines
1171 and definitions for research on epithelial-mesenchymal transition. *Nat Rev Mol Cell Biol.*
1172 2020;21:341-352.

1173 **100.** Tang N, Marshall WF, McMahon M, Metzger RJ, Martin GR. Control of mitotic spindle
1174 angle by the RAS-regulated ERK1/2 pathway determines lung tube shape. *Science.*
1175 2011;333:342-345.

1176 **101.** Tang N, Marshall WF. Centrosome positioning in vertebrate development. *J Cell Sci.*
1177 2012;125:4951-4961.

1178 **102.** Quijada P, Trembley MA, Small EM. The Role of the Epicardium During Heart
1179 Development and Repair. *Circ Res.* 2020;126:377-394.

1180 **103.** Batlle E, Wilkinson DG. Molecular mechanisms of cell segregation and boundary
1181 formation in development and tumorigenesis. *Cold Spring Harb Perspect Biol.*
1182 2012;4:a008227.

1183 **104.** LeGoff L, Lecuit T. Mechanical Forces and Growth in Animal Tissues. *Cold Spring Harb*
1184 *Perspect Biol.* 2015;8:a019232.

1185 **105.** Lim HYG, Plachta N. Cytoskeletal control of early mammalian development. *Nat Rev*
1186 *Mol Cell Biol.* 2021;22:548-562.

1187 **106.** de Gooijer MC, van den Top A, Bockaj I, Beijnen JH, Wurdinger T, van Tellingen O.
1188 The G2 checkpoint-a node-based molecular switch. *FEBS Open Bio.* 2017;7:439-455.

1189 **107.** Musacchio A, Salmon ED. The spindle-assembly checkpoint in space and time. *Nat Rev*
1190 *Mol Cell Biol.* 2007;8:379-393.

1191 **108.** Nakaseko Y, Yanagida M. Cell biology. Cytoskeleton in the cell cycle. *Nature.*
1192 2001;412:291-292.

1193 **109.** Jones MC, Zha J, Humphries MJ. Connections between the cell cycle, cell adhesion and
1194 the cytoskeleton. *Philos Trans R Soc Lond B Biol Sci.* 2019;374:20180227.

1195 **110.** Gachet Y, Tournier S, Millar JB, Hyams JS. A MAP kinase-dependent actin checkpoint
1196 ensures proper spindle orientation in fission yeast. *Nature.* 2001;412:352-355.

1197 **111.** Lee K, Song K. Actin dysfunction activates ERK1/2 and delays entry into mitosis in
1198 mammalian cells. *Cell Cycle.* 2007;6:1487-1495.

1199 **112.** Shrestha D, Choi D, Song K. Actin Dysfunction Induces Cell Cycle Delay at G2/M with
1200 Sustained ERK and RSK Activation in IMR-90 Normal Human Fibroblasts. *Mol Cells.*
1201 2018;41:436-443.

1202 **113.** Yan Y, Black CP, Cowan KH. Irradiation-induced G2/M checkpoint response requires
1203 ERK1/2 activation. *Oncogene.* 2007;26:4689-4698.

1204 **114.** Yan Y, Hein AL, Greer PM, Wang Z, Kolb RH, Batra SK, Cowan KH. A novel function
1205 of HER2/Neu in the activation of G2/M checkpoint in response to gamma-irradiation.
1206 *Oncogene.* 2015;34:2215-2226.

1207 **115.** Deschenes-Simard X, Kottakis F, Meloche S, Ferbeyre G. ERKs in cancer: friends or
1208 foes? *Cancer Res.* 2014;74:412-419.

1209 **116.** Lin Z, von Gise A, Zhou P, Gu F, Ma Q, Jiang J, Yau AL, Buck JN, Gouin KA, van Gorp
1210 PR, Zhou B, Chen J, Seidman JG, Wang DZ, Pu WT. Cardiac-specific YAP activation
1211 improves cardiac function and survival in an experimental murine MI model. *Circ Res.*
1212 2014;115:354-363.

1213 **117.** von Gise A, Pu WT. Endocardial and epicardial epithelial to mesenchymal transitions in
1214 heart development and disease. *Circ Res.* 2012;110:1628-1645.

1215 **118.** Morikawa Y, Zhang M, Heallen T, Leach J, Tao G, Xiao Y, Bai Y, Li W, Willerson JT,
1216 Martin JF. Actin cytoskeletal remodeling with protrusion formation is essential for heart
1217 regeneration in Hippo-deficient mice. *Sci Signal.* 2015;8:ra41.

1218 **119.** Kodo K, Ong SG, Jahanbani F, Termglinchan V, Hirono K, InanlooRahatloo K, Ebert
1219 AD, Shukla P, Abilez OJ, Churko JM, Karakikes I, Jung G, Ichida F, Wu SM, Snyder
1220 MP, Bernstein D, Wu JC. iPSC-derived cardiomyocytes reveal abnormal TGF-beta
1221 signalling in left ventricular non-compaction cardiomyopathy. *Nat Cell Biol.*
1222 2016;18:1031-1042.

1223 **120.** D'Amato G, Luxan G, del Monte-Nieto G, Martinez-Poveda B, Torroja C, Walter W,
1224 Bochter MS, Benedito R, Cole S, Martinez F, Hadjantonakis AK, Uemura A, Jimenez-
1225 Borreguero LJ, de la Pompa JL. Sequential Notch activation regulates ventricular
1226 chamber development. *Nat Cell Biol.* 2016;18:7-20.

1227 **121.** Luxan G, Casanova JC, Martinez-Poveda B, Prados B, D'Amato G, MacGrogan D,
1228 Gonzalez-Rajal A, Dobarro D, Torroja C, Martinez F, Izquierdo-Garcia JL, Fernandez-
1229 Friera L, Sabater-Molina M, Kong YY, Pizarro G, Ibanez B, Medrano C, Garcia-Pavia
1230 P, Gimeno JR, Monserrat L, Jimenez-Borreguero LJ, de la Pompa JL. Mutations in the
1231 NOTCH pathway regulator MIB1 cause left ventricular noncompaction cardiomyopathy.
1232 *Nat Med.* 2013;19:193-201.

1233 **122.** Faber JW, D'Silva A, Christoffels VM, Jensen B. Lack of morphometric evidence for
1234 ventricular compaction in humans. *J Cardiol.* 2021;78:397-405.

1235